Riemann surface approach to bound and resonant states: Exotic resonant states for a central rectangular potential

Cornelia Grama, N. Grama, and I. Zamfirescu
Institute of Atomic Physics, P.O.Box MG-6, Bucharest, Romania
(Received 8 March 1999; published 16 February 2000)

An approach to bound and resonant states in scattering by a central potential $gV(r)$, $g \in \mathbb{C}$, based on a global analysis of *S*-matrix poles, is presented. The global method involves the construction of the Riemann surface $R_g^{(l)}$ over the g plane on which the pole function $k=k^{(l)}(g)$ is single valued and analytic. This implies the division of the Riemann surface $R_g^{(l)}$ into sheets and the construction of the Riemann sheets images in the k plane. By keeping the sheets of the Riemann surface apart, the single pole laying on each sheet image in the k plane is identified. With each state (l,n) of the quantum system one associates a sheet $\Sigma_n^{(l)}$ of the Riemann surface $R_g^{(l)}$. A new quantum number n with a topological meaning is introduced in order to label a pole and the corresponding state (l,n). All *S*-matrix poles for a central rectangular potential $gV(r)$, with $l=0$, 1, 2, 3, and 4, are analyzed by using the global method. A new class of resonant state poles, having unusual properties, is identified. The properties of these resonant state poles (exotic poles) and of the corresponding resonant states are studied. A new type of resonance in the cross section, associated with the cooperative contribution from three adjacent partial waves and due to the local degeneracy with respect to l, is discussed.

PACS number(s): 03.65.Nk, 34.50.−s, 34.80.Bm

I. INTRODUCTION

The resonant structures in the cross section of many interesting phenomena, such as field ionization, photoionization, electron scattering on atoms and molecules, and nuclear scattering are, in most cases, ascribed to resonant states of the quantum-system. An adequate quantum mechanical description of the resonant states is of importance in many branches of physics, because general laws of formation and decay of long-lived states in molecules, atoms, nuclei, condensed matter, and hadronic collisions are necessary. The most fundamental approach to resonant scattering is through the analytic properties of the *S* matrix [1–3].

We consider nonrelativistic scattering by a central potential $gV(r)$, $g \in \mathbb{C}$. The poles of the *S* matrix are the solutions $k=k^{(l)}(g)$ of the equation

$$\mathcal{F}_{l+}(g,k)=0, \tag{1.1}$$

provided that $\mathcal{F}_{l-}(g,k)\neq 0$. Here $\mathcal{F}_{l+}(g,k)$ and $\mathcal{F}_{l-}(g,k)$ are the denominator and numerator, respectively, of the *S*-matrix element S_l [1]. $\mathcal{F}_{l+}(g,k)$ is the Jost function, g is the potential strength, k is the wave number, and l is the orbital angular momentum. The pole function $k=k^{(l)}(g)$ is a multiple-valued function defined on the complex g plane.

Due to their close connection to bound and resonant states, sometimes referred to as Gamow states or Siegert states, the poles of the *S* matrix have been extensively studied [4–11]. *S*-matrix poles have been studied not only in the usual scattering process, but also in scattering process in an external field [12,13]. The pole distribution in the k plane as a function of the potential strength g has been investigated for various potentials by a combination of graphical, numerical, and asymptotic methods in many papers, for example Refs. [14–26]. In all the above-mentioned papers a particular path in the complex g plane has been chosen, and corresponding trajectories of the *S*-matrix poles in the k plane have been determined. In the following this method will be called the ''pole trajectory method.'' Resonant state poles found by the pole trajectory method have familiar properties: (i) They become bound or virtual state poles when the depth of the potential well is increased, i.e., $|k|\to\infty$ for $|g|\to\infty$. (ii) The corresponding resonant states have wave functions confined to the well region. These poles will be called ''old-class resonant state poles.'' In the pole trajectory method only a poor description of the function $k=k^{(l)}(g)$ is obtained. One can never be sure that all the poles in the k plane have been found because one makes a particular choice of the path in the complex g plane. Moreover, by using the pole trajectory method one can never be sure that the same pole is followed. For example, recently contradictory opinions have been raised relative to the *S*-matrix poles trajectories in the complex k plane for a complex square potential. Dąbrowski [25] claimed that the statements of Gal *et al.* [27], Oset *et al.* [28], and Bonetti *et al.* [29], concerning the dependence of the *S*-matrix poles location in the k plane on the strength of the absorptive potential, were not correct, and proposed a general rule for the movement of a pole with increasing $\mathrm{Re}\, g$ and $\mathrm{Im}\, g$. In fact the pole trajectory method does not allow a definite answer to this question, as will be shown in the present paper.

In order to have a complete description of the *S*-matrix poles in the k plane, a global analysis of the function $k=k^{(l)}(g)$ is necessary. In the present paper a Riemann surface approach to bound and resonant states in the case of scattering by a central potential $gV(r)$, $g \in \mathbb{C}$, based on a global analysis of the function $k=k^{(l)}(g)$, is presented. The construction of the Riemann surface $R_g^{(l)}$ for a central rectangular potential with $l=0$, 1, 2, 3, and 4 is given in detail. A construction of the images of the Riemann sheets in the k plane is also done.

The paper is organized as follows: In Sec. II a global method for analysis of all *S*-matrix poles for various classes

of potentials $gV(r)$ is discussed. The Riemann surface of the pole function $k=k^{(l)}(g)$ for a central rectangular potential with $l=0-4$ is constructed in Sec. III. In this case analytic expressions of the branch points and stable points are obtained in Secs. III A and III B, respectively. In Sec. III C the sheets $\Sigma_n^{(l)}$ of the Riemann surface $R_g^{(l)}$ and their images $\Sigma_n'^{(l)}$ in the k plane are analyzed for each l value in the range $l=0-4$. By using the global analysis of all S-matrix poles, a new class of resonant state poles is identified on some Riemann sheet images. Because of their unusual properties the new-class resonant state poles are also called ''exotic resonant state poles,'' and their corresponding resonant states are called ''exotic resonant states.'' The properties of the Riemann sheets $\Sigma_n^{(l)}$ and of their k-plane images $\Sigma_n'^{(l)}$ that follow from this analysis are summarized in Sec. III D. In Sec. III E the properties of the exotic resonant states are discussed. In Sec. IV a summary of the results is given.

Although the distribution of the S-matrix poles for a central rectangular potential was studied in several papers [18–20] the new-class resonant state poles (exotic poles) have not been identified because only a global method allows for the identification of all S-matrix poles. The shortcomings of the previous analyses are stressed in more detail in Sec. III, where the Riemann surface is constructed for each orbital angular momentum. The usual manner of studying resonant states prevented theoreticians from identifying the new class of resonant states. For example, many authors determined the energies and wave functions of the resonant states by solving the Schrödinger equation for real energies (see, e.g., Ref. [30]). They defined the energy of the resonant state as the energy where the ratio of the maximum amplitude of the wave-function inside the potential well over the wave function amplitude at large distances is at a maximum. By using this definition of the resonant states these authors restricted themselves from the very beginning to the old class of resonant states. On the other hand, authors who studied the S-matrix pole trajectories in the k plane followed only particular paths in the complex g plane, and in this way they lost the new-class of resonant state poles (e.g., see Ref. [20]).

The global analysis of all S-matrix poles for a central rectangular potential can be used as a guide for the global analysis of all S-matrix poles for other potential shapes. In Ref. [31] the Riemann surface for a potential made of a central rectangular or Woods-Saxon well plus Coulomb barrier has been constructed. For this potential the description of the Riemann surface and the arrangement of the proper connections between sheets are complicated. It was not possible to obtain analytic expressions for the branch points, but only asymptotic approximations for the large Sommerfeld parameter. For a central rectangular potential with a Coulomb barrier there is a countable infinity of cuts in the g plane that accumulate on the real g axis, which renders the separation of the Riemann sheets difficult. It was the investigation of the case of a central rectangular potential with large orbital angular momentum that allowed an understanding of the structure of the more complicated case of a central rectangular potential with a Coulomb barrier. This is why it is important to construct the Riemann surface $R_g^{(l)}$ for a central rectangular potential not only for a low orbital angular momentum, but also for large orbital angular momenta.

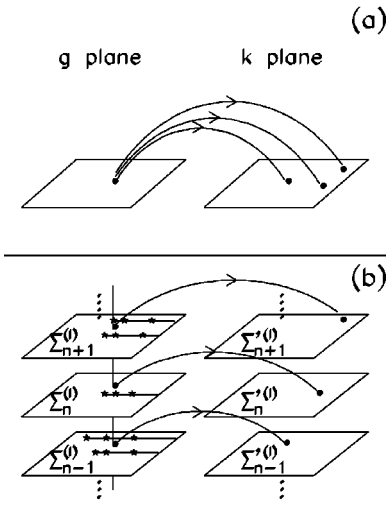

FIG. 1. (a) The multiple-valued function $k=k^{(l)}(g)$ defined on the complex g plane. (b) The Riemann surface $R_g^{(l)}$ over the complex g plane of the function $k=k^{(l)}(g)$. Sheets $\Sigma_n^{(l)}$ of the Riemann surface $R_g^{(l)}$ and their k-plane images $\Sigma_n'^{(l)}$ are shown. The branch points denoted by * and the branch lines that join the branch points are indicated. One can see that if g takes a value on a sheet $\Sigma_n^{(l)}$, then the function $k=k^{(l)}(g)$ takes only one value on the image of this sheet, $\Sigma_n'^{(l)}$.

II. GLOBAL METHOD FOR ALL *S*-MATRIX POLES ANALYSIS

The global method for all S-matrix poles analysis involves the construction of the Riemann surface $R_g^{(l)}$ over the g plane on which the pole function $k=k^{(l)}(g)$ is single valued and analytic. This implies the division of the Riemann surface $R_g^{(l)}$ into sheets, and the construction of Riemann sheet images in the k plane. By keeping the sheets of the Riemann surface apart, the single pole laying on each sheet image in the k plane is identified. In this way all the poles are identified and no pole is lost. A schematic illustration of the method is given in Fig. 1. In Fig. 1(a) the function $k=k^{(l)}(g)$ defined on the complex g plane is multiple valued, i.e., there are many k values that correspond to a given g value. In Fig. 1(b) the function $k=k^{(l)}(g)$ defined on the Riemann surface $R_g^{(l)}$ is single valued. If g takes a value on a sheet $\Sigma_n^{(l)}$, then the function $k=k^{(l)}(g)$ takes only one value on the image of this sheet $\Sigma_n'^{(l)}$, or, in other words, there is only a single pole on each sheet image. Moreover, if g takes values on a continuous path on a given Riemann sheet $\Sigma_n^{(l)}$, then its image $k=k^{(l)}(g)$ takes values on a continuous path on the Riemann sheet image $\Sigma_n'^{(l)}$.

The global method is a powerful tool in S-matrix pole analysis because it reduces the analysis of an infinity of poles in the k plane to the analysis of a single pole on each Riemann sheet image in the k plane. In this way each pole is separated and analyzed.

The main step in the construction of the Riemann surface $R_g^{(l)}$ is to find the branch points of the function $k=k^{(l)}(g)$. According to the implicit function theory [32,33], the singular points g_i of the function $k^{(l)}(g)$ are the solutions of the system

$$\mathcal{F}_{l+}(g,k)=0, \tag{2.1a}$$

$$\frac{\partial \mathcal{F}_{l+}(g,k)}{\partial k}=0. \tag{2.1b}$$

From among these singular points g_i, those that are branch points may be found by permitting the variable g to describe successive small circuits round each singular point g_i, and by observing whether the function $k^{(l)}(g)$ returns to its initial value. Let $m>1$ be the smallest number of rotations after which one again obtains the initial value of the function $k^{(l)}(g)$. Then g_i is a branch point of order $m-1$, and m sheets of the Riemann surface $R_g^{(l)}$ are joined at this point.

The border of any sheet image in the k plane $\Sigma_n'^{(l)}$ is obtained by letting g trace a path along the cuts on the corresponding Riemann sheet $\Sigma_n^{(l)}$, without crossing them, and along a circle of large radius joining the cuts. On each sheet image there is only one pole. This pole and the corresponding resonant (bound) state are labeled by a pair of quantum numbers l and n, where the number n is the label of the Riemann sheet image $\Sigma_n'^{(l)}$ on which the pole is situated. The sheets and their images are to be ordered in a conventional way.

Because it is impossible to obtain analytical expressions of the branch points as a function of the potential parameters for a whole class of potentials, the construction of the Riemann surface has to be done for each case individually. The global method may also be used in the case of the multichannel scattering. In this case g is the potential strength in one of the channels.

A. Finite range potential

The equation $\mathcal{F}_{l+}(g,k)=0$ defines the implicit function $k=k^{(l)}(g)$. The Jost function $\mathcal{F}_{l+}(g,k)$ is entire in g and k for several classes of potentials. One of them is formed of the finite range potentials $gV(r)$ which satisfy the following properties [34]:

(1) $\int_0^\infty r|V(r)|dr<\infty$.

(2) $V(r)=0$ for $r>R$, where R is a fixed positive radius.

(3) $V(r)$ has an asymptotic expansion about the point $r=R$, whose first term is $V(r)\approx C(1-r/R)^\sigma$ with $\sigma\geqslant 0$.

(4) $V(r)$ is continuous and has continuous derivatives up to some order $>\sigma$ for all r in the range $0<r<R$.

A second class of potentials having the entire Jost function in g and k is made of potentials piecewise continuous with piecewise continuous derivatives up to some order [35]. A third class of potentials with the entire Jost function in g and k consists of potentials which decrease faster than all exponentials [1].

Julia [36] and Stoilow [37] studied the domain of existence and the properties of an implicit function $y=y(x)$ defined by an irreducible relation $G(x,y)=0$, where $G(x,y)$ is an entire function with respect to x and y. By using their results the following properties of $k=k^{(l)}(g)$ for the abovementioned classes of potentials are obtained.

(P1) There is a Riemann surface $R_g^{(l)}$ over the g plane on which $k^{(l)}(g)$ is a single-valued and analytic function. The boundary of $R_g^{(l)}$ is the set E [the points g for which the equation $\mathcal{F}_{l+}(g,k)=0$ has no solution in k].

(P2) $k^{(l)}(g)$ has at most a countable infinity of branches, i.e., the Riemann surface $R_g^{(l)}$ has at most a countable infinity of sheets covering the g plane.

(P3) $k^{(l)}(g)$ and its inverse function have Iversen's property, i.e., these functions can be continued analytically from an arbitrary point to another arbitrary point along a curve which lies in a given neighborhood of a prescribed curve joining these points. In this case the Riemann surface $R_g^{(l)}$ is of class $\mathcal{I}$ (Iversen).

(P4) If $g\in R_g^{(l)}$ and $g_i\in E$, and if $g\to g_i$ then $k^{(l)}(g)\to\infty$.

(P5) Set E is at most a countable infinite set having infinity as the unique limit point, i.e., it is discontinuous everywhere. This follows from the Iversen property.

For a fixed g $(g\neq 0)$, the Jost function $\mathcal{F}_{l+}(g,k)$ of a finite range potential $gV(r)$ has a countable infinity of zeros of finite order [34], and the Riemann surface $R_g^{(l)}$ has a countable infinity of sheets. The boundary set of the Riemann surface has a single element $E=\{g=0\}$, i.e., Eq. (1.1) has no solution in k for $g=0$. When $g\to 0$ the S-matrix poles go to infinity (i.e., $k\to\infty$). These properties are particular cases of the general properties P2, P5, and P4, respectively.

Because the Jost function $\mathcal{F}_{l+}(g,k)$ is entire in g and k, it can be factorized in the form [38]

$$\mathcal{F}_{l+}(g,k)=e^{G(g,k)}\prod_{n=1}^{\infty}[f_n(g,k)]^{\alpha_n}e^{Q_n(g,k)}, \tag{2.2}$$

where $G(g,k)$ and $f_n(g,k)$ are entire functions, α_n is a positive integer, and $Q_n(g,k)$ is a polynomial. Moreover, the roots of the system,

$$f_n(g,k)=0, \tag{2.3a}$$

$$\frac{\partial f_n(g,k)}{\partial k}=0, \tag{2.3b}$$

are isolated in $\mathbb{C}\times\mathbb{C}$ [38]. According to Eqs. (2.2) and (2.3) the singular points and, therefore, the branch points of the Riemann surface $R_g^{(l)}$ are discrete.

B. Other classes of potentials

The global method for all S-matrix poles analysis, based on the construction of the Riemann surface $R_g^{(l)}$, can be used not only for finite range potentials but also for other classes of potentials, for which the Jost function is analytic in a particular domain of the k plane. Construction of the Riemann surface follows the same procedure. For each particular case the domain of analyticity in the k plane must be determined. In Ref. [31] the global method for all S-matrix poles analysis has been used in the case of a Woods-Saxon potential with a Coulomb barrier. In this case the Jost func-

tion $\mathcal{F}_{l+}(g,k)$ is analytic in k in the domain $D(k)=\mathrm{Im}\,k>-a$, except the origin $k=0$ and the negative imaginary axis, where it has a cut. Here $a=(2d)^{-1}$, where d is the diffuseness of the Woods-Saxon potential. In this case the sheet images of $R_g^{(l)}$ in the k plane have been studied, except for a narrow strip containing the origin $k=0$ and the negative imaginary axis. In Ref. [31] a new class of poles and resonant states was found. It was shown that the quasimolecular states populated in the heavy-ion scattering are a particular case of such exotic resonant states. The properties of the quasimolecular states [energy, width, deviation from the linear dependence of the energy on $l(l+1)$, doorway character, and criteria for observability] result in a natural way from the general properties of the exotic resonant states.

III. RIEMANN SURFACE $R_g^{(l)}$ OF THE FUNCTION $k=k^{(l)}(g)$ FOR A CENTRAL RECTANGULAR POTENTIAL

The central rectangular potential

$$\frac{2mR^2}{\hbar^2}gV(r)=\begin{cases}-g & \text{for } r/R\leqslant 1, \quad g\in\mathbb{C}\\ 0 & \text{for } r/R>1\end{cases} \tag{3.1}$$

is a particular case of a finite range potential and, consequently, its Jost function $\mathcal{F}_{l+}(g,k)$ is entire in g and k. We will use the dimensionless variable r/R rather than the variable r. For the sake of simplicity, in the following the notation k will be used for the dimensionless variable kR.

The Jost function of potential (3.1) is [18]

$$\mathcal{F}_{l+}(g,k)=\left(\frac{k}{k_0}\right)^l W_l(g,k), \tag{3.2}$$

where

$$W_l(g,k)=w_l(k,R)u_l'(k_0,R)-\frac{k}{k_0}w_l'(k,R)u_l(k_0,R) \tag{3.3}$$

is the Wronskian at $r=R$ of the reduced radial wave functions $w_l(k,r)=krh_l^{(1)}(kr)$ and $u_l(k_0,r)=k_0rj_l(k_0r)$, valid for $r\geqslant R$ and $r<R$, respectively. Here $h_l^{(1)}(kr)$ is the spherical Hankel function of the first kind, $j_l(k_0r)$ is the spherical Bessel function [39], and $k_0=(k^2+g)^{1/2}$. The prime in Eq. (3.3) indicates the differentiation with respect to the argument of the function. Because $k=0$ is an exceptional point (it is not a pole of the S matrix) [1], we use the equation

$$W_l(g,k)=0, \tag{3.4}$$

rather than Eq. (1.1) to define the S-matrix poles. In order to find the branch points it is easier to use the system made of Eq. (3.4) and the equation

$$\frac{\partial W_l(g,k)}{\partial k}=0 \tag{3.5}$$

than the system of equations (2.1a) and (2.1b).

A. Branch points

The branch points have been found by solving the system of equations (3.4) and (3.5). By using the recurrence relations [39]

$$\frac{l+1}{z}f_l(z)+\frac{d}{dz}f_l(z)=f_{l-1}(z), \quad l\neq 0, \tag{3.6a}$$

$$\frac{l}{z}f_l(z)-\frac{d}{dz}f_l(z)=f_{l+1}(z), \tag{3.6b}$$

where $f_l(z)$ denotes the spherical Bessel function $j_l(z)$ or the spherical Hankel function of the first kind $h_l^{(1)}(z)$, the system of equations (3.4) and (3.5) becomes

$$h_{l+1}^{(1)}(k)=0, \tag{3.7a}$$

$$j_{l+1}(k_0)=0, \tag{3.7b}$$

or

$$h_{l-1}^{(1)}(k)=0, \quad l\neq 0, \tag{3.8a}$$

$$j_{l-1}(k_0)=0, \quad l\neq 0. \tag{3.8b}$$

According to Eqs. (3.7) and (3.8) the branch points of the function $k=k^{(l)}(g)$ are

$$g_{s,s'}^{+}=x_{l+1,s}^2-y_{l+1,s'}^2, \tag{3.9}$$

$$g_{s,s'}^{-}=x_{l-1,s}^2-y_{l-1,s'}^2, \quad l\neq 0, \tag{3.10}$$

where $x_{m,s}$ $(s=1,2,\ldots)$ are the zeros of the spherical Bessel functions $j_m(z)$, and $y_{m,s'}$ $(s'=1,2,\ldots,m)$ are the zeros of the spherical Hankel functions of the first kind $h_m^{(1)}(z)$, respectively. According to Eqs. (3.9) and (3.10) there is a countable infinity of branch points for a given value of l, because the functions $j_{l\pm1}(k_0)$ have a countable infinity of real simple zeros. These branch points have a finite number of images in the k plane due to the fact that $h_{l+1}^{(1)}$ and $h_{l-1}^{(1)}$ have a finite number of complex simple zeros. The zeros of the Bessel and Hankel functions have been extensively investigated. Asymptotic approximations of large zeros and of zeros for large orders are very well known [39]. Using the zeros of $j_{l\pm1}$ and $h_{l\pm1}^{(1)}$ tabulated in Refs. [39] and [40], respectively, the branch points have been calculated.

In order to show that the branch points (3.9) and (3.10) are of order 1, the derivatives $\partial W_l(g,k)/\partial g$ and $\partial^2 W_l(g,k)/\partial k^2$ at the branch points are to be calculated. From Eqs. (3.3), (3.9), and (3.10), using the recurrence relations (3.6a) and (3.6b), it results that

$$\frac{\partial W_l(g_{s,s'}^{+},y_{l+1,s'})}{\partial g}=\frac{1}{2}h_l^{(1)}(y_{l+1,s'})j_{l+1}'(x_{l+1,s})\neq 0, \tag{3.11}$$

$$\frac{\partial W_l(g^-_{s,s'},y_{l-1,s'})}{\partial g}=\frac{1}{2}h_l^{(1)}(y_{l-1,s'})j'_{l-1}(x_{l-1,s})\neq 0, \quad l\neq 0, \tag{3.12}$$

$$\frac{\partial^2 W_l(g^+_{s,s'},y_{l+1,s'})}{\partial k^2}=-\frac{(2l+1)g^+_{s,s'}}{(x_{l+1,s})^2}\times h_l^{(1)}(y_{l+1,s'})j_l(x_{l+1,s})\neq 0, \tag{3.13}$$

$$\frac{\partial^2 W_l(g^-_{s,s'},y_{l-1,s'})}{\partial k^2}=\frac{(2l-1)g^-_{s,s'}}{(x_{l-1,s})^2}\times h_l^{(1)}(y_{l-1,s'})j_l(x_{l-1,s})\neq 0, \quad l\neq 0. \tag{3.14}$$

Taking into account that the values $\partial W_l(g,k)/\partial g$ and $\partial^2 W_l(g,k)/\partial k^2$ at the branch points are different from zero, it results that $d^2k/dg^2\neq 0$, i.e., the branch points (3.9) and (3.10) are of order 1.

Besides the just mentioned algebraic branch points, there is a transcendental branch point at $g=0$. Indeed, let us determine the form of the function $k=k^{(l)}(g)$ in the neighborhood of $g=0$. For $g=0$, from Eq. (3.3) one obtains $W(0,k)=-1/k^2$, which is different from zero for any finite k, i.e., Eq. (3.4) has no solution in k for $g=0$. Consequently $g=0$ is the only element of the boundary set E. According to property P4,

$$\lim_{g\to 0} k^{(l)}(g)=\infty, \tag{3.15}$$

so that there are only large roots of Eq. (3.4) for $g\to 0$. Using the asymptotic expansions of j_l and $h_l^{(1)}$ for large arguments [39], it results that the large roots of Eq. (3.4) are solutions of the equation

$$\exp(2ik)=-(-1)^l 4k^2/g. \tag{3.16}$$

The roots of Eq. (3.16) for any $g\in\mathbb{C}$ were studied in detail by Wright [41]. Based on the results of Ref. [41], the roots of Eq. (3.4) for $g\to 0$ are obtained:

$$k\sim\begin{cases}\pi n-\dfrac{1}{2}(\arg g-i\ln|g|) & \text{for even } l\\ \pi(n+1/2)-\dfrac{1}{2}(\arg g-i\ln|g|) & \text{for odd } l,\end{cases} \tag{3.17}$$

where $n=0,\pm 1,\pm 2,\ldots$ and $0\leqslant\arg g<2\pi$. Therefore, the transcendental branch point $g=0$ is a logarithmic branch point whose order is infinite, and consequently all the sheets of the Riemann surface $R_g^{(l)}$ are joined together at $g=0$. The number n from Eq. (3.17) will be used in order to label the Riemann sheets $\Sigma_n^{(l)}$ and their k-plane images $\Sigma_n'^{(l)}$. Moreover, n will be used as a new quantum number to label the pole belonging to sheet image $\Sigma_n'^{(l)}$ and the corresponding quantum state (l,n). This quantum number is completely different in kind from l, which is connected to the rotational invariance, while n has a topological meaning.

B. Stable points

The asymptotic approximation of the solutions $k=k^{(l)}(g)$ of Eq. (3.4) for large g will be investigated in order to show that some poles remain at a finite distance as $g\to\infty$. In other words, there are some poles that remain in bound regions of the k plane for $|g|\to\infty$. Taking into account the asymptotic expansion of the spherical Bessel function $j_l(k_0)$ for large g [39], and using the recurrence relation (3.6b), from Eq. (3.4) we obtain

$$h_l^{(1)}(k)+\epsilon k h_{l+1}^{(1)}(k)=0, \tag{3.18}$$

where $\epsilon=-[\sqrt{g}\cot(\sqrt{g}-l\pi/2)]^{-1}$ is a small quantity ($\epsilon\to 0$) if g is complex and $|g|\to\infty$. By using the relation $h_l^{(1)}(k)=-i(e^{ik}/k^{l+1})\theta_l(-ik)$ [42], where θ_l is the Bessel polynomial defined by the relation

$$\theta_l(z)=\sum_{m=0}^{l}\frac{(l+m)!}{(l-m)!m!}\frac{1}{2^m}z^{l-m}, \tag{3.19}$$

Eq. (3.18) becomes

$$\theta_l(-ik)-\epsilon\theta_{l+1}(-ik)=0. \tag{3.20}$$

This is a polynomial equation which has $l+1$ roots for $\epsilon\neq 0$ and l roots for $\epsilon=0$. The roots of Bessel polynomials are simple roots [42]. We determine the asymptotic expansion of the $l+1$ roots of Eq. (3.20) as $\epsilon\to 0$, i.e., $|g|\to\infty$, by using the method presented in Ref. [43]. One obtains

$$k^{(l,n)}=\kappa_n^{(l)}(1+\epsilon), \quad n=1,2,\ldots,l \tag{3.21}$$

and

$$k^{(l,l+1)}=-i/\epsilon, \tag{3.22}$$

where $-i\kappa_n^{(l)}$ $(n=1,2,\ldots,l)$ are the roots of the Bessel polynomials $\theta_l(z)$, i.e., $\theta_l(-i\kappa_n^{(l)})=0$. In other words, for a given complex g, $|g|\to\infty$, there are l poles, namely, $k^{(l,n)}$ $(n=1,2,\ldots,l)$, that remain at finite distance according to Eq. (3.21). Indeed, we have

$$\lim_{g\to\infty} k^{(l,n)}=\kappa_n^{(l)}, \quad n=1,2,\ldots,l, \tag{3.23}$$

provided g is complex. Taking this into account we call $\kappa_n^{(l)}$ $(n=1,2,\ldots,l)$ ''stable points.'' From Eq. (3.23) it results that the stable points act as attractors for these l poles.

According to the behavior for $|g|\to\infty$, two classes of poles can be distinguished. Some poles behave in the familiar way, i.e., $|k|\to\infty$ for $|g|\to\infty$, [see Eq. (3.22)]. These poles belong to the old class of resonant state poles. As shown by Eq. (3.23), for each l there are l poles that remain

at finite distance, in the neighborhood of the stable points, when $|g|\to\infty$. These poles belong to the new class of poles (exotic resonant state poles).

Due to the above-mentioned connection between the Bessel polynomials $\theta_l(-ik)$ and the spherical Hankel function of the first kind $h_l^{(1)}(k)$, it results that the stable point $\kappa_n^{(l)}$ is a zero of the spherical Hankel function of the first kind, i.e., $h_l^{(1)}(\kappa_n^{(l)})=0$ for $n=1,2,\ldots,l$. The zeros of the spherical Hankel functions of the first kind are symmetrically distributed with respect to the imaginary k axis, along a half-eye-shaped curve in the lower k half-plane [44]. This means that for odd l there is a zero of $h_l^{(1)}(k)$ on the imaginary k axis, and $(l-1)/2$ zeros in the fourth quadrant of the k plane. For even l there are $l/2$ zeros of $h_l^{(1)}$ in the fourth quadrant of the k plane. By convention, in the following the stable points in the fourth quadrant will be ordered according to increasing $\mathrm{Re}\,k$.

C. Analysis of the Riemann surface $R_g^{(l)}$ for $l=0-4$

According to Eqs. (3.9) and (3.10) there is a countable infinity of algebraic branch points $g_{s,s'}^{\pm}$ for a given l because the spherical Bessel functions $j_{l\pm1}(k_0)$ have a countable infinity of real simple zeros. These branch points $g_{s,s'}^{\pm}$ have a finite number of images $k(g_{s,s'}^{\pm})$ in the k plane due to the fact that $h_{l+1}^{(1)}(k)$ and $h_{l-1}^{(1)}(k)$ have a finite number of simple complex zeros. The zeros $x_{l\pm1,s}$, $(s=1,2,\ldots)$ of the spherical Bessel functions are real, and the zeros $y_{l\pm1,s'}$ $(s'=1,2,\ldots,l\pm1)$ of the spherical Hankel function of the first kind are complex, so that the algebraic branch points for a given l can be grouped into sets characterized by the same $\mathrm{Im}\,g$. Consequently the cuts that allow a separation of the Riemann sheets have been taken by joining the branch points with the same $\mathrm{Im}\,g$ by rectilinear segments going to $\mathrm{Re}\,g\to\infty$. Besides these cuts there is a cut along the positive real g axis starting at the transcendental branch point $g=0$. To summarize, there are $2l+1$ cuts for odd l, $2l-1$ cuts for even l $(l\neq0)$, and one cut on the positive real g axis for $l=0$. All the algebraic branch points are of order 1, so that at a given algebraic branch point only two sheets are joined together. One determines the sheets that are joined at a given algebraic branch point $g_{s,s'}^{\pm}$ by taking successive small circuits $|g-g_{s,s'}^{\pm}|=\rho$ round the given branch point $g_{s,s'}^{\pm}$. Let us start with $g=g_i\in\Sigma_n^{(l)}$ and $k_i=k^{(l)}(g_i)\in\Sigma_n'^{(l)}$. After a complete rotation of g round the branch point $g_{s,s'}^{\pm}$, the pole reaches another value $k=k_f\in\Sigma_m'^{(l)}$. After a second complete rotation of g, the pole reaches again its initial value $k_i\in\Sigma_n'^{(l)}$. It results that $g_{s,s'}^{\pm}$ is a branch point where sheets $\Sigma_n^{(l)}$ and $\Sigma_m^{(l)}$ are joined together. A more detailed discussion will be done for each value of the orbital momentum l in the corresponding subsections. The order of the transcendental branch point $g=0$ is infinite, so that all the sheets are joined at $g=0$. The number n from Eq. (3.17) will be used in order to label the Riemann sheets $\Sigma_n^{(l)}$ and their k-plane images $\Sigma_n'^{(l)}$. Moreover, n will be used as a new quantum number to label the pole belonging to sheet image $\Sigma_n'^{(l)}$ and the corresponding quantum state (l,n). In the analysis of the Riemann surface $R_g^{(l)}$ the property [1]

$$\mathcal{F}_l(g,k)=\mathcal{F}_l^*(g^*,-k^*) \tag{3.24}$$

of the Jost function will be used.

TABLE I. The branch points $g_{s,s'}^{+}$ in the case $l=0$. The zeros of the spherical Bessel function $j_1(k_0)$ are denoted by $k_{0,s}^{+}$. $k_{s'}$ $(s'=1)$ stands for the zero of the spherical Hankel function of the first kind $h_1^{(1)}(k)$.

s'	s	$k_{0,s}^{+}$	$k_{s'}$	$g_{s,1}^{+}$
1	1	4.493	$-i$	21.191
1	2	7.725	$-i$	60.679
1	3	10.904	$-i$	119.900
⋮	⋮	⋮	⋮	⋮
1	n	$\sim(n+1/2)\pi$	$-i$	$\sim1+(n+1/2)^2\pi^2$

1. Case $l=0$

The S-matrix poles are solutions $k=k^{(0)}(g)$ of Eq. (3.4) which can be written as

$$ik=k_0\cot k_0, \tag{3.25}$$

where $k_0=(g+k^2)^{1/2}$. Let us construct the Riemann surface $R_g^{(0)}$ over the g plane, on which the function $k=k^{(0)}(g)$ is single valued and analytic. For $l=0$ system (3.7) becomes

$$h_1^{(1)}(k)=-\frac{i+k}{k^2}e^{ik}=0, \tag{3.26}$$

$$j_1(k_0)=\frac{\sin k_0-k_0\cos k_0}{k_0^2}=0. \tag{3.27}$$

The branch points of the Riemann surface $R_g^{(0)}$ are given by Eq. (3.9) for $l=0$ where $y_{1,s'}$ and $x_{1,s}$ are the solutions of the Eqs. (3.26) and (3.27), respectively.

Let $k_{s'}$ $(s'=1)$ be the zero of $h_1^{(1)}(z)$ and $k_{0,s}^{+}$ $(s=1,2,\ldots)$ be the zeros of $j_1(z)$. With the values $k_1=-i$ given by Eq. (3.26) and $k_{0,s}^{+}$ given by Eq. (3.27), the branch points $g_{s,s'}^{+}$ are obtained from Eq. (3.9):

$$g_{s,1}^{+}=(k_{0,s}^{+})^2-k_1^2, \quad s=1,2,\ldots. \tag{3.28}$$

It results that, in addition to the logarithmic branch point $g=0$, there is a countable infinity of branch points on the real axis, given by Eq. (3.28) and presented in Table I.

The Riemann surface $R_g^{(0)}$ will be constructed according to the usual procedure: a cut is taken in the g plane, joining all branch points by a simple line. The rest of the domain is simple conex. In the present case there is only one cut, namely, the cut along the half-axis $[0,+\infty)$. To each branch of the multivalued function $k^{(0)}(g)$ a sheet of the Riemann surface $R_g^{(0)}$ is associated. We label the sheets and their k-plane images by the integer $n=0,\pm1,\pm2,\ldots$ which oc-

curs in Eq. (3.17), that defines the pole for $g \to 0$. Set E of boundary points has only one point, namely, $g=0$. For $g \in \Sigma_n^{(0)}$ the corresponding pole is situated on $\Sigma'^{(0)}_n$. The border of each sheet $\Sigma_n^{(0)}$ is obtained by varying g along the two edges of the cut $[0,\infty)$ and on a circle of a large radius joining them. The border of the k-plane sheet image $\Sigma'^{(0)}_n$ is obtained by following the pole defined by Eq. (3.25), when g describes the border of $\Sigma_n^{(0)}$.

The sheets $\Sigma_0^{(0)}$, $\Sigma_1^{(0)}$, $\Sigma_2^{(0)}$, and $\Sigma_3^{(0)}$, as well as their k-plane images $\Sigma'^{(0)}_0$, $\Sigma'^{(0)}_1$, $\Sigma'^{(0)}_2$, and $\Sigma'^{(0)}_3$, respectively, are represented in Fig. 2. In order to describe these sheets and their k-plane images, a detailed construction of their borders will be given in the following.

We start the construction of each sheet border at the point $g=0$. For $g \to 0$, $g \in \Sigma_0^{(0)}$, the pole on $\Sigma'^{(0)}_0$ is situated at $k \sim -\frac{1}{2}(\arg g - i \ln|g|)$ [see Eq. (3.17)]. Point A in Fig. 2(b) indicates the position of the pole for $g=+i\varepsilon$, where $\varepsilon > 0$ (ε small), i.e., for $\arg g = \pi/2$. When the potential strength g increases along the upper edge of the cut $[0,\infty)$ on the sheet $\Sigma_0^{(0)}$ (a more and more attractive potential), this pole moves upwards along the negative imaginary k axis, and passes through $k=-i$ at $g=1$, crossing the origin for $g=(\pi/2)^2$. For $g>(\pi/2)^2$ it becomes a bound state pole, giving rise to the first bound state (ground state). For $g \in \Sigma_0^{(0)}$, $g=-i\varepsilon$, i.e., for $\arg g = 3\pi/2$, the pole is situated in the point denoted by G in Fig. 2(b). When $\mathrm{Re}\, g$ increases so that g moves on the sheet $\Sigma_0^{(0)}$ along the lower edge of the cut $[0,\infty)$, the pole approaches the straight line $\mathrm{Re}\, k = -\pi$; then it moves upwards until it approaches the straight line $\mathrm{Im}\, k = -1$. When $\mathrm{Re}\, g$ increases further, the pole approaches the imaginary k axis. The pole passes through $k=-i$ at $g=21.191$; then it becomes a virtual pole, moving toward $k=-i\infty$ as $g \to \infty$.

Similarly, for $g \to 0$, $g \in \Sigma_1^{(0)}$, the pole on $\Sigma'^{(0)}_1$ is situated at $k \sim \pi - \frac{1}{2}(\arg g - i \ln|g|)$. Points A and G in Fig. 2(d) indicate the position of this pole for $g=+i\varepsilon$ and $g=-i\varepsilon$, respectively. When the potential strength g increases on sheet $\Sigma_1^{(0)}$ along the upper edge of the cut $[0,\infty)$ the pole approaches the straight line $\mathrm{Re}\, k = \pi$; then it moves upwards until it approaches the straight line $\mathrm{Im}\, k = -1$. The pole then moves toward the imaginary k axis, passes through $k=-i$ at $g=21.191$, and then becomes a virtual pole, moving toward $k=-i\infty$ as $g \to \infty$. When the potential strength g increases on sheet $\Sigma_1^{(0)}$ along the lower edge of the cut $[0,\infty)$ the pole starting from point G in Fig. 2(d) moves upwards along the negative imaginary k axis, and passes through $k=-i$ at $g=1$, crossing the origin for $g=(\pi/2)^2$. For $g>(\pi/2)^2$ it becomes a bound state pole.

For $g \to 0$, $g \in \Sigma_2^{(0)}$, the pole on $\Sigma'^{(0)}_2$ is situated at $k \sim 2\pi - \frac{1}{2}(\arg g - i \ln|g|)$. For $g \to 0$, $g \in \Sigma_3^{(0)}$ the pole on $\Sigma'^{(0)}_3$ is situated at $k \sim 3\pi - \frac{1}{2}(\arg g - i \ln|g|)$. In Figs. 2(f) and 2(h) point A denotes the position of the pole on the sheet images $\Sigma'^{(0)}_2$ and $\Sigma'^{(0)}_3$ for g taking the value $g=+i\varepsilon$ on sheets $\Sigma_2^{(0)}$ and $\Sigma_3^{(0)}$, respectively. Similarly, point G denotes the position of the pole on sheet images $\Sigma'^{(0)}_2$ and $\Sigma'^{(0)}_3$ for g taking the value $g=-i\varepsilon$ on sheets $\Sigma_2^{(0)}$ and $\Sigma_3^{(0)}$, respectively. When the potential strength g is increased on $\Sigma_2^{(0)}$ along the upper edge of the cut $[0,\infty)$, the pole starting from point A on $\Sigma'^{(0)}_2$ reaches $k=-i$ for $g=60.679$, and then becomes a virtual state pole. When the potential strength is increased on the sheet $\Sigma_2^{(0)}$ from $g=0$ to $g \to \infty$ along the lower edge of the cut $[0,\infty)$, the pole starting from point G on $\Sigma'^{(0)}_2$ reaches $k=-i$ for $g=21.191$, then

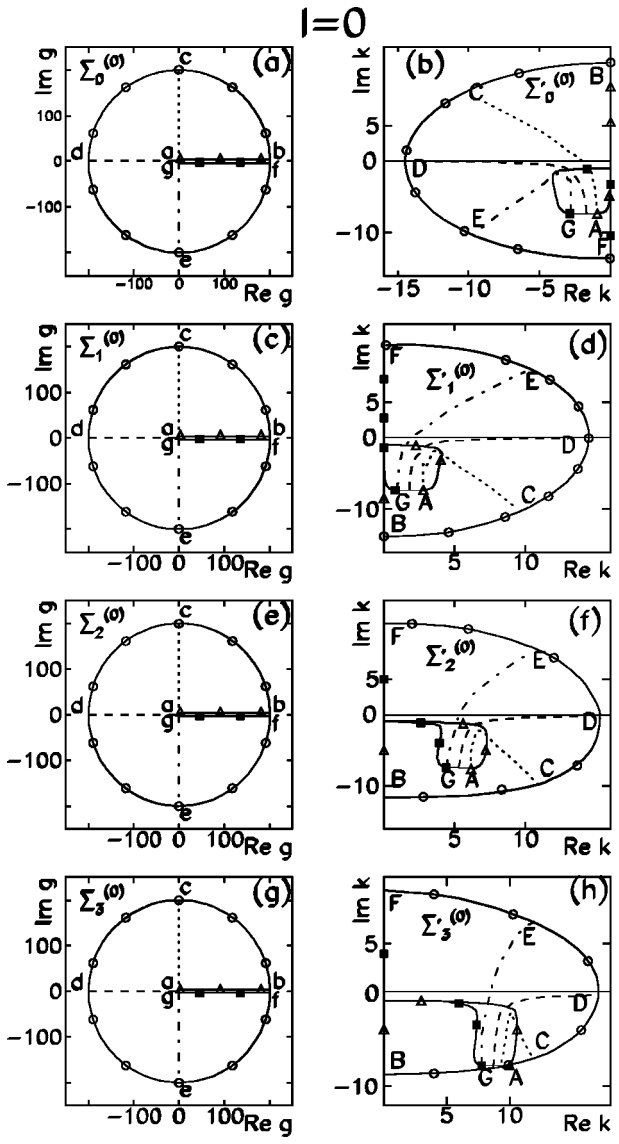

FIG. 2. Sheets $\Sigma_n^{(0)}$ ($n=0,1,2,3$) of the Riemann surface $R_g^{(0)}$ and their k-plane images $\Sigma'^{(0)}_n$ for a central rectangular potential with $l=0$. The borders of the sheets, made of the edges of the cut $[0,\infty)$ and a circle of a large radius, are shown in (a), (c), (e), and (g). The k-plane images of the Riemann sheet borders are shown in (b), (d), (f), and (h), respectively. Different symbols are used in order to indicate the two edges of the cut and the large radius circle in the g plane. The k-plane image of the corresponding sheet border segment is marked by the same symbol. We denote A, B, C, . . . the k-plane images of the points a, b, c, . . . from the g plane. By dashed, dotted, and dash-dotted lines a pure real barrier, a pure absorptive potential, and a pure emissive potential, respectively, are indicated.

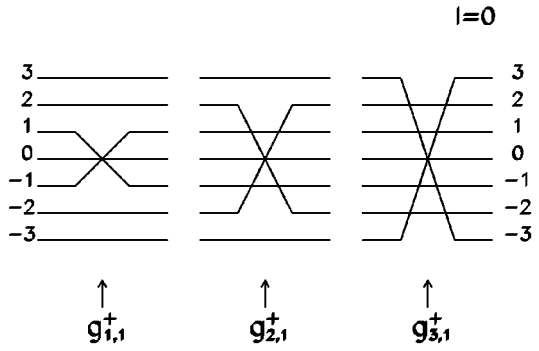

FIG. 3. The junctions of sheets $\Sigma_n^{(0)}$ and $\Sigma_m^{(0)}$ $(n,m=0,\pm1,\pm2,\pm3)$ for a central rectangular potential with $l=0$ at the branch points $g_{s,1}^+$, $(s=1,2,3)$. The label n or m of each sheet is indicated by the numbers given at the left and right ends of the picture. One can see, for example, that for $g=g_{1,1}^+$ sheet $\Sigma_{-1}^{(0)}$ is joined to sheet $\Sigma_1^{(0)}$.

moves upwards along the imaginary k axis and becomes a bound state pole. Similarly, on sheet image $\Sigma_3'^{(0)}$ the pole starting from point A reaches $k=-i$ for $g=119.900$, while the pole starting from point G reaches $k=-i$ at $g=60.679$.

When $g\to\infty$ on sheet $\Sigma_s^{(0)}$ $(s=1,2,3,\ldots)$, the pole goes to $k\to-i\infty$ on $\Sigma_s'^{(0)}$ if g follows the upper edge of the cut $[0,\infty)$, and to $k\to i\infty$ if g follows the lower edge of the cut $[0,\infty)$. When $g\to\infty$ on sheet $\Sigma_{-s}^{(0)}$ $(s=1,2,3,\ldots)$ the pole goes to $k\to i\infty$ on $\Sigma_{-s}'^{(0)}$ if g follows the upper edge of the cut $[0,\infty)$, and to $k\to-i\infty$ if g follows the lower edge of the cut $[0,\infty)$. For $s=1,2,\ldots$, sheet image $\Sigma_{-s}'^{(0)}$ is symmetric to sheet image $\Sigma_{s+1}'^{(0)}$ with respect to the imaginary k axis.

The analysis of the sheets shows that at each branch point $g_{s,1}^+$ sheets $\Sigma_{-s}^{(0)}$ and $\Sigma_s^{(0)}$, $s=1,2,\ldots$, are joined. In Fig. 3 the way the sheets are joined at the branch points is schematically shown. We remark that sheet $\Sigma_0^{(0)}$ (the ground-state sheet) has no junction with any other sheet if the potential is present $(g\neq0)$. We remind the reader that at $g=0$ all the sheets are joined together.

A comparison of the present results in the case $l=0$ with the results obtained in the previous analyses stresses the advantage of the global method. Indeed, Nussenzveig [18] studied the case of a real potential. He showed that complex poles approach from opposite sides the imaginary k axis at $k=-i$, where the S matrix has a double pole, obtained for a potential strength $g=g_{s,1}^+$ in our notation (see Fig. 1 of Ref. [18]). For $g>g_{s,1}^+$ the double pole splits into a pair of poles which move in opposite directions along the imaginary k axis. However, due to the fact that Ref. [18] did not use a global analysis, one cannot specify which of the initial poles becomes a bound state pole $(\mathrm{Im}\,k>0)$ and which one becomes a virtual state pole $(\mathrm{Im}\,k<0)$. On the contrary, when using the global method for pole analysis, once a Riemann sheet is chosen there is one and only one pole on the corresponding k-plane image of the sheet, and this pole can be followed when the potential strength changes. This can be clearly seen from Fig. 2. The trajectories of the S-matrix poles for a central complex rectangular potential well were calculated by Joffily [19] by choosing given paths in the complex g plane. In Ref. [19] pole trajectories for a purely absorptive imaginary well and for a complex absorptive well with a given ratio between real and imaginary parts of the potential strength have been calculated. However, as the pole equation has infinitely many roots for an arbitrary g, one cannot specify which pole has been found by graphical methods and iterative processes. On the k plane it is possible to jump involuntarily from one pole to the other. Conversely, the global method allows the identification of each pole. In other words, if we have two points on a given sheet image we can pass from one to another, being sure that we follow the same pole. Recently contradictory opinions have been given relative to the effect of the absorptive part of the potential strength on the pole location. Does the virtual state pole move clockwise into the third quadrant of the k plane, or counterclockwise into the fourth quadrant? This question was differently answered in Refs. [27–29] and [25]. In fact it is not possible to give a definite answer by using the pole trajectory method. From Fig. 2 one can see that the answer depends on the sheet image on which the pole is situated: on sheet images $\Sigma_0'^{(0)}$, $\Sigma_{-1}'^{(0)}$, $\Sigma_{-2}'^{(0)}$, ... the pole moves into the third quadrant, while on sheet images $\Sigma_1'^{(0)}$, $\Sigma_2'^{(0)}$, ... it moves into the fourth quadrant when the absorption is switched on. In connection with the analysis given in Ref. [25], we should also note that two poles are associated with the same state (2s), for the same potential strength. This is an erroneous result, because one should associate a single pole with each state. In our analysis the 2s state is associated with the pole (0,1), situated on the sheet image $\Sigma_1'^{(0)}$.

2. Case l=1

For $l=1$ the pole equation (3.4) can be written

$$\frac{ik^2-k-i}{k+i}=\frac{(k_0^2-1)\sin k_0+k_0\cos k_0}{\sin k_0-k_0\cos k_0}. \tag{3.29}$$

The branch points of the Riemann surface are given by the system of equations (3.9) and (3.10), where $x_{l\pm1,s}$ and $y_{l\pm1,s'}$ are the solutions of Eqs. (3.7) and (3.8) taken for $l=1$. As $h_0^{(1)}(z)=e^{iz}/z$ has no zero, it results that the branch points are determined only by Eq. (3.9). For $l=1$ the system of equation (3.7) can be written

$$h_2^{(1)}(k)=\frac{ie^{ik}}{k}\left[1+\frac{3i}{k}-\frac{3}{k^2}\right]=0, \tag{3.30}$$

$$j_2(k_0)=-\frac{3\cos k_0}{k_0^2}+\frac{(3-k_0^2)\sin k_0}{k_0^3}=0. \tag{3.31}$$

From these equations the k-plane images of the branch points $k_{s'}$ $(s'=1,2)$,

$$k_{1,2}=\frac{1}{2}(\pm\sqrt{3}-3i), \tag{3.32}$$

and the zeros $k_{0,s}^+$ $(s=1,2,3,\ldots)$ of the spherical Bessel function $j_2(k_0)$ are obtained. From Eq. (3.9) the following branch points result:

TABLE II. The branch points $g^+_{s,s'}$ in the case $l=1$. The zeros of the spherical Bessel functions $j_2(k_0)$ are denoted by $k^+_{0,s}$. $k_{s'}$ $(s'=1,2)$ stand for the zeros of the spherical Hankel function of the first kind $h^{(1)}_2(k)$.

s'	s	$k^+_{0,s}$	$k_{s'}$	$g^+_{s,s'}$
1	1	5.763	$0.866-1.500i$	$34.717+2.598i$
1	2	9.909	$0.866-1.500i$	$84.219+2.598i$
1	3	12.322	$0.866-1.500i$	$153.355+2.598i$
⋮	⋮	⋮	⋮	⋮
1	n	$\sim(n+1)\pi$	$\sqrt{3}/2-3i/2$	$\sim(n+1)^2\pi^2-k_1^2$
2	1	5.763	$-0.866-1.500i$	$34.717-2.598i$
2	2	9.909	$-0.866-1.500i$	$84.219-2.598i$
2	3	12.322	$-0.866-1.500i$	$153.355-2.598i$
⋮	⋮	⋮	⋮	⋮
2	n	$\sim(n+1)\pi$	$-\sqrt{3}/2-3i/2$	$\sim(n+1)^2\pi^2-k_2^2$

$$g^+_{s,1}=(k^+_{0,s})^2-k_1^2=(k^+_{0,s})^2+\frac{3}{2}(1+i\sqrt{3}) \qquad (3.33)$$

and

$$g^+_{s,2}=(k^+_{0,s})^2-k_2^2=(k^+_{0,s})^2+\frac{3}{2}(1-i\sqrt{3}), \qquad (3.34)$$

where $s=1,2,\ldots$. In Table II the values of these branch points and of their k-plane images are given. One can see that besides the logarithmic branch point $g=0$ there are two infinite sets of branch points $g^+_{s,s'}$, ($s'=1$ and 2 and $s=1,2,3,\ldots$). Each set is characterized by the same $\mathrm{Im}\, g^+_{s,s'}$.

The Riemann surface will be constructed by taking two cuts in the g plane, parallel to the real axis. These cuts join all the complex branch points of the function $k=k^{(1)}(g)$. A cut along the positive real g axis will also be taken. The rest of the domain is simple conex. Proceeding in the same manner as in the case $l=0$, sheets of the Riemann surface $R^{(1)}_g$ are constructed. Sheet $\Sigma^{(1)}_0$ is joined with sheet $\Sigma^{(1)}_s$ at the branch point $g^+_{s,1}$, and sheet $\Sigma^{(1)}_0$ is joined with sheet $\Sigma^{(1)}_{-s}$ at the branch point $g^+_{s,2}$, where $s=1,2,3,\ldots$. The situation is illustrated in Fig. 4, where the way the sheets are joined one to another is shown for the branch points $g^+_{s,1}$, with $s=1$, 2, and 3.

In Fig. 5 sheets $\Sigma^{(1)}_0$, $\Sigma^{(1)}_1$, and $\Sigma^{(1)}_2$ and their k-plane images are represented. One observes that a large part of sheet $\Sigma^{(1)}_0$, namely, the region with $\mathrm{Re}\, g>\mathrm{Re}\, g^+_{1,1}$ and $\mathrm{Im}\, g>\mathrm{Im}\, g^+_{s,1}$, is mapped by the function $k=k^{(1)}(g)$ onto a bound region of the k-plane sheet image $\Sigma'^{(1)}_0$. This region, indicated by hatching in Fig. 5(b), lies on the branch point image $k_1=\sqrt{3}/2-3i/2$ and on the stable point $\kappa^{(1)}_1=-i$, defined as the solution of equation $h^{(1)}_1(k)=0$. Another large part of the sheet $\Sigma^{(1)}_0$, namely, the region with $\mathrm{Re}\, g>\mathrm{Re}\, g^+_{1,2}$ and $\mathrm{Im}\, g<\mathrm{Im}\, g^+_{s,2}$, is mapped by the function $k=k^{(1)}(g)$ onto another bound region of $\Sigma'^{(1)}_0$ that lies on the branch point image $k_2=-\sqrt{3}/2-3i/2$ and on the same stable point. Details on the bound regions of the sheet image $\Sigma'^{(1)}_0$ are shown in Fig. 5(c). If the potential strength g on $\Sigma^{(1)}_0$ is situated in the windows of the potential strength $\mathrm{Im}\, g>\mathrm{Im}\, g^+_{s,1}=3\sqrt{3}/2$ or $\mathrm{Im}\, g<\mathrm{Im}\, g^+_{s,2}=-3\sqrt{3}/2$, the corresponding pole belongs to the new class of poles, i.e., it remains in a bound region of the k plane and does not become a bound or virtual state pole when the depth of the potential well increases indefinitely ($\mathrm{Re}\, g\to\infty$). This is an exotic resonant state pole. From Fig. 5 one can see that the Riemann sheet image $\Sigma'^{(1)}_0$ does not include the positive imaginary k axis, or, in other words, the pole on $\Sigma'^{(1)}_0$ cannot become a bound state pole. Moreover, if $|\mathrm{Im}\, g|>|\mathrm{Im}\, g^+_{s,s'}|=3\sqrt{3}/2$, the regions where the exotic poles are located shrink to the stable point for a sufficiently deep potential well, according to Eq. (3.23). In other words the stable point is an attractor for the exotic resonant state pole, which is insensitive to the behavior of the potential in the internal region (well region). In Fig. 6 the trajectory of the pole on $\Sigma'^{(1)}_0$ is shown for g varying as $g=\lambda(10+i)$, where λ takes values between 3.5 and 500. One can see the spiral asymptotic trajectory of the exotic resonant state pole approaching the stable point $\kappa^{(1)}_1=-i$. If $|\mathrm{Im}\, g|<|\mathrm{Im}\, g^+_{s,s'}|=3\sqrt{3}/2$ on $\Sigma^{(1)}_0$, then the corresponding pole on $\Sigma'^{(1)}_0$ belongs to the old class of poles, i.e., the pole behaves in a familiar way when the potential strength increases. Indeed, when $\mathrm{Re}\, g$ increases, the pole moves toward the imaginary k axis and becomes a virtual state pole for a sufficiently deep potential well.

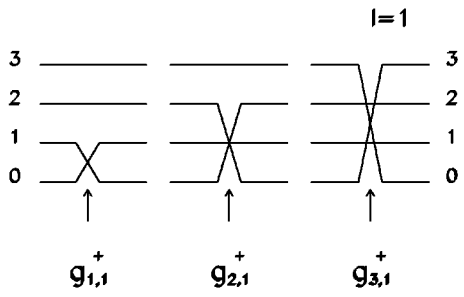

FIG. 4. The junctions of sheets $\Sigma^{(1)}_n$ and $\Sigma^{(1)}_m$ $(n,m=0,1,2,3)$ for a central rectangular potential with $l=1$ at the branch points $g^+_{s,1}$ $(s=1,2,3)$. The label n or m of each sheet is indicated by the number given at the left and right ends of the picture.

Sheet $\Sigma^{(1)}_1$ and its k-plane image are represented in Figs. 5(d) and 5(e), respectively. One can see that on sheet image $\Sigma'^{(1)}_1$ there is only an old-class resonant state pole. The bound region of the k plane where the exotic resonant state pole was located on $\Sigma'^{(1)}_0$ is empty on $\Sigma'^{(1)}_1$. This means that the pole trajectories on $\Sigma'^{(1)}_1$, corresponding to any path of g on $\Sigma^{(1)}_1$ that does not cross the cuts, avoid the region of the k plane where the exotic resonant state pole was located on sheet image $\Sigma'^{(1)}_0$.

On the next Riemann sheet images $\Sigma'^{(1)}_s$, $(s=2,3,\ldots)$ there are only old-class poles. The boundaries of these sheet images can be constructed starting from the position of the

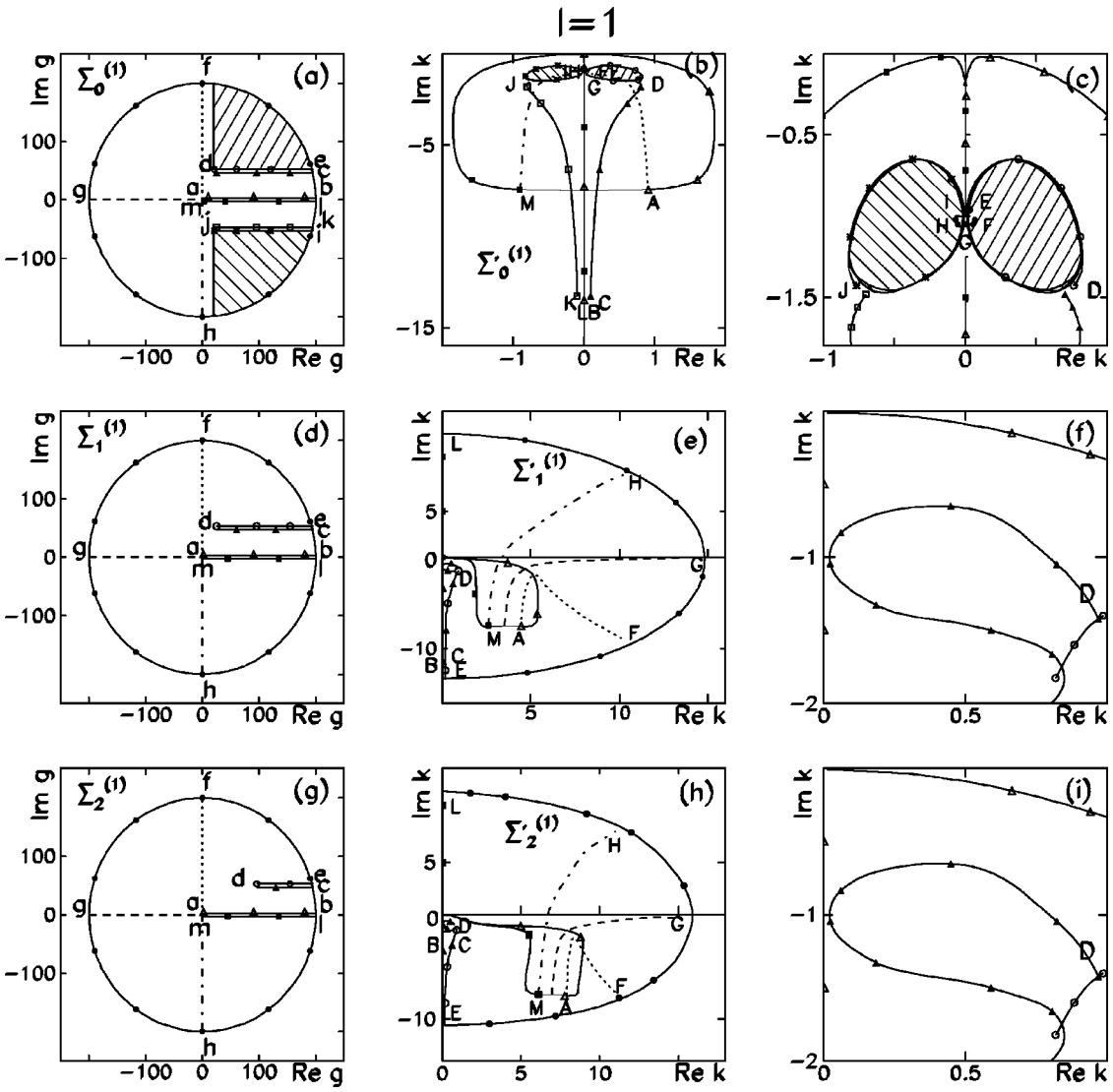

FIG. 5. Sheets $\Sigma_n^{(1)}$ $(n=0,1,2)$ of the Riemann surface $R_g^{(1)}$ and their k-plane images $\Sigma_n'^{(1)}$ for a central rectangular potential with $l=1$. The borders of the sheets, made of the edges of the cut $[0,\infty)$, the edges of the cuts that join the complex branch points, and a circle of a large radius are shown in (a), (d), and (g). The k-plane images of the sheet borders are given in (b), (e), and (h). Details of the Riemann sheet images $\Sigma_n'^{(1)}$ $(n=0,1,2)$ are shown in (c), (f), and (i). Different symbols are used in order to indicate the two edges of each cut and the large radius circle in the g plane. The k-plane image of the corresponding sheet border segment is marked by the same symbol. By A, B, C, ..., we denote the k-plane images of the points a, b, c, ... from the g plane. The hatched regions of sheet $\Sigma_0^{(1)}$ are mapped by the function $k=k^{(1)}(g)$ onto the bound regions of $\Sigma_0'^{(1)}$ indicated by the same hatching. In each of these bound regions of $\Sigma_0'^{(1)}$ the exotic resonant state pole is situated. One can see that the region occupied by the exotic resonant state pole on $\Sigma_0'^{(1)}$ is empty on sheet images $\Sigma_1'^{(1)}$ and $\Sigma_2'^{(1)}$; i.e., the poles on $\Sigma_1'^{(1)}$ and $\Sigma_2'^{(1)}$ cannot be situated in this region.

pole for $g=0$. On all these sheet images the bound region of the k plane where the exotic resonant state pole was located on $\Sigma_0'^{(1)}$ is empty.

Sheets $\Sigma_{-s}^{(1)}$ and $\Sigma_s^{(1)}$ $(s=1,2,\ldots)$ are symmetric with respect to the real g axis. According to the property (3.24) of the Jost function, the k-plane images $\Sigma_{-s}'^{(1)}$ and $\Sigma_s'^{(1)}$ $(s=1,2,\ldots)$ are symmetric with respect to the imaginary k axis.

In Ref. [20] the pole distribution for a real square well and $l=1$ has been studied. The exotic resonant state pole, i.e., the pole that is located in the bound region between the stable point $k=-i$ and the branch point image $k=\sqrt{3}/2-3i/2$, has not been found in the quoted paper, due to the nonglobal treatment of the pole function. Similarly, in Ref. [25] the effect of the absorptive part of the potential on the pole location was analyzed by the pole trajectory method. The exotic pole was not found, because the path chosen for the potential strength did not enter the hatched region in Fig. 2(a). In Ref. [25] there are two poles associated with the same state $(1p)$ for the same potential strength. This is an erroneous result, because one should associate a single pole with each state. In our analysis the $1p$ state is associated

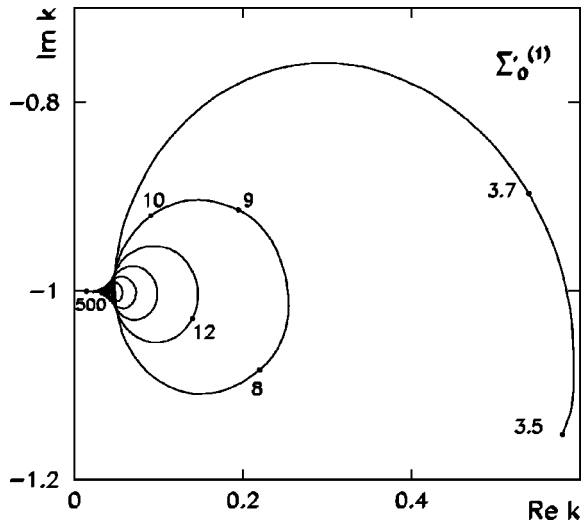

FIG. 6. The trajectory of the exotic resonant state pole on sheet image $\Sigma_0'^{(1)}$ for g varying as $g=\lambda(10+i)$, where λ takes values in the range 3.5–500. The numbers beside the spiral curve give the λ values.

with pole (1,0), situated on sheet image $\Sigma_0'^{(1)}$.

3. Case l=2

For $l=2$ the pole equation (3.4) becomes

$$\frac{k^3+3ik^2-6k-6i}{ik^2-3k-3i}=\frac{(3k_0^2-6)\sin k_0-(k_0^3-6k_0)\cos k_0}{(k_0^2-3)\sin k_0+3k_0\cos k_0}. \tag{3.35}$$

The branch points of the Riemann surface are given by the system of equations (3.9) and (3.10), where $x_{l\pm1,s}$ and $y_{l\pm1,s'}$ are the solutions of the system of equations (3.7) and (3.8), which in the case $l=2$ can be written as

$$h_3^{(1)}(k)=-\frac{ie^{ik}}{k^4}[15-15ik-6k^2+ik^3]=0, \tag{3.36a}$$

$$j_3(k_0)=\frac{1}{k_0^4}[(15-6k_0^2)\sin k_0+k_0(k_0^2-15)\cos k_0]=0 \tag{3.36b}$$

and

$$h_1^{(1)}(k)=-\frac{i+k}{k^2}e^{ik}=0, \tag{3.36c}$$

$$j_1(k_0)=\frac{\sin k_0-k_0\cos k_0}{k_0^2}=0, \tag{3.36d}$$

respectively. In other words the k-plane images of the branch points are given by the zero of $h_1^{(1)}(k)$ and the zeros of $h_3^{(1)}(k)$. Using Eqs. (3.9) and (3.10), four sets of branch points have been obtained, corresponding to $k_{0,s}^{\pm}$, ($s=1,2,3,\ldots$) taking values from the infinite set of zeros of the spherical Bessel functions $j_1(k_0)$ and $j_3(k_0)$ and to $k_{s'}$ ($s'=1,2,3,4$) taking values from the finite set of zeros of the spherical Hankel functions of the first kind $h_1^{(1)}(k)$ and $h_3^{(1)}(k)$. In Table III the algebraic branch points $g_{s,s'}^{\pm}$ and their images in the k plane are presented.

TABLE III. The branch points in the case $l=2$. The zeros of the spherical Bessel functions $j_1(k_0)$ and $j_3(k_0)$, respectively, are denoted by $k_{0,s}^-$ and $k_{0,s}^+$. $k_{s'}$ ($s'=1$) stands for the zero of the spherical Hankel function of the first kind $h_1^{(1)}(k)$, and $k_{s'}$ ($s'=2,3,4$) stand for the zeros of the spherical Hankel function of the first kind $h_3^{(1)}(k)$.

s'	s	$k_{0,s}^-$	$k_{s'}$	$g_{s,s'}^-$
1	1	4.493	$-1.000i$	21.191
1	2	7.725	$-1.000i$	60.680
1	3	10.904	$-1.000i$	119.900
⋮	⋮	⋮	⋮	⋮
1	n	$\sim(n+1/2)\pi$	$-1.000i$	$\sim(n+1/2)^2\pi^2-k_1^2$
s'	s	$k_{0,s}^+$	$k_{s'}$	$g_{s,s'}^+$
2	1	6.988	$-2.322i$	54.224
2	2	10.417	$-2.322i$	113.909
2	3	13.698	$-2.322i$	193.028
⋮	⋮	⋮	⋮	⋮
2	n	$\sim(n+3/2)\pi$	$-2.322i$	$\sim(n+3/2)^2\pi^2-k_2^2$
3	1	6.988	$-1.754-1.839i$	$49.135-6.452i$
3	2	10.417	$-1.754-1.839i$	$108.820-6.452i$
3	3	13.698	$-1.754-1.839i$	$187.940-6.452i$
⋮	⋮	⋮	⋮	⋮
3	n	$\sim(n+3/2)\pi$	$-1.754-1.839i$	$\sim(n+3/2)^2\pi^2-k_3^2$
4	1	6.988	$1.754-1.839i$	$49.135+6.452i$
4	2	10.417	$1.754-1.839i$	$108.820+6.452i$
4	3	13.698	$1.754-1.839i$	$187.940+6.452i$
⋮	⋮	⋮	⋮	⋮
4	n	$\sim(n+3/2)\pi$	$1.754-1.839i$	$\sim(n+3/2)^2\pi^2-k_4^2$

Two of the four infinite sets of branch points are real, and the other two are characterized by $\mathrm{Im}\, g_{s,s'}^+=\pm6.452$. By using the procedure described in the preamble of Sec. III C the Riemann surface $R_g^{(2)}$ was constructed. Let $s=1,2,3,\ldots$. Sheet $\Sigma_0^{(2)}$ is joined to sheet $\Sigma_s^{(2)}$ at the branch points $g_{s,1}^-$ and $g_{s,2}^+$. Sheet $\Sigma_{-s+1}^{(2)}$ is joined to sheet $\Sigma_{-s}^{(2)}$ at the branch point $g_{s,3}^+$. Sheet $\Sigma_s^{(2)}$ is joined to sheet $\Sigma_{s+1}^{(2)}$ at the branch point $g_{s,4}^+$. The way the sheets are joined is shown schematically in Fig. 7. For simplicity, only the junctions of sheets $\Sigma_n^{(2)}$ and $\Sigma_m^{(2)}$ with $n,m\geqslant0$ are shown.

In Fig. 8 the Riemann sheets $\Sigma_1^{(2)}$ and $\Sigma_2^{(2)}$, as well as their k-plane images $\Sigma_1'^{(2)}$ and $\Sigma_2'^{(2)}$, are shown. One observes that a large part of sheet $\Sigma_1^{(2)}$, namely, the region with $\mathrm{Re}\, g>\mathrm{Re}\, g_{s,4}^+$ and $\mathrm{Im}\, g>\mathrm{Im}\, g_{s,4}^+$, is mapped by the function $k=k^{(2)}(g)$ onto a bound region of the k-plane sheet image $\Sigma_1'^{(2)}$ that lies on the branch point image $k_4=1.754-1.839i$ and on the stable point $\kappa_1^{(2)}=\sqrt{3}/2-3i/2$ [the solution of the equation $h_2^{(1)}(k)=0$]. Another large part

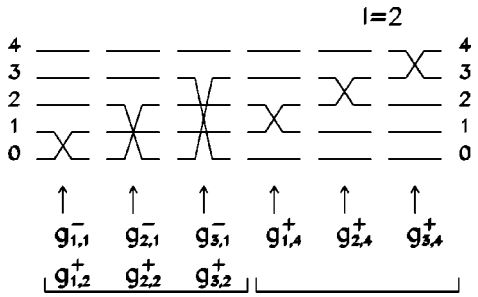

FIG. 7. The junctions of sheets $\Sigma_n^{(2)}$ and $\Sigma_m^{(2)}$ $(n,m=0,1,2,3,4)$ for a central rectangular potential with $l=2$ at the branch points $g^-_{s,1}$, $g^+_{s,2}$, $g^+_{s,3}$, and $g^+_{s,4}$ $(s=1,2,3)$. The label n or m of each sheet is indicated by the numbers given at the left and right ends of the picture.

of the sheet $\Sigma_1^{(2)}$, namely, the region with $\mathrm{Re}\, g>0$ and $\mathrm{Im}\, g<0$, is mapped by the function $k=k^{(2)}(g)$ onto another bound region of the k plane that lies on the branch point images $k_1=-i$ and $k_2=-2.322i$ and on the same stable point $\kappa_1^{(2)}=\sqrt{3}/2-3i/2$. Details of Fig. 8(b) are given in Fig. 8(c), where the bound regions of the sheet image $\Sigma_1'^{(2)}$ are shown at an enlarged scale. The pole situated on sheet image $\Sigma_1'^{(2)}$ that corresponds to a potential well of strength g with $0<\mathrm{Im}\, g<\mathrm{Im}\, g^+_{s,4}=6.452$ behaves in a familiar way when the potential strength increases: it moves toward the imaginary k axis and for a sufficiently deep well becomes a virtual pole. The pole situated on sheet image $\Sigma_1'^{(2)}$, that corresponds to a potential strength g with $\mathrm{Im}\, g>\mathrm{Im}\, g^+_{s,4}=6.452$ or $\mathrm{Im}\, g<0$, is an exotic resonant state pole. It behaves in an unusual way: the pole does not become a bound or virtual state pole as the potential strength g increases, but remains in a bound region of the k plane. The border of the bound region of the k plane, where the exotic resonant state pole is situated, lies on a pair of points: a stable point and the k-plane image of a branch point. When the potential strength increases to infinity the exotic resonant state pole approaches the stable point [see Eq. (3.23)].

Sheet $\Sigma_2^{(2)}$ and its k-plane image are represented in Figs. 8(d) and 8(e), respectively. One can see that there is only an old-class pole on this sheet image. The region of the k plane where the exotic resonant state pole was located on $\Sigma_1'^{(2)}$ is empty on $\Sigma_2'^{(2)}$.

Sheet $\Sigma_0^{(2)}$ is symmetric to sheet $\Sigma_1^{(2)}$ with respect to the real g axis and its k-plane image $\Sigma_0'^{(2)}$ is, according to the Jost function property, symmetric with respect to the imaginary k axis to image $\Sigma_1'^{(2)}$. Consequently sheet $\Sigma_0^{(2)}$ and its image $\Sigma_0'^{(2)}$ are not shown in Fig. 8, although on sheet image $\Sigma_0'^{(2)}$ there are two bound regions in the third quadrant of the k plane where the exotic resonant state pole that corresponds to a strongly emissive potential $(\mathrm{Im}\, g<-\mathrm{Im}\, g^+_{s,4})$ or to an absorptive potential $(\mathrm{Im}\, g>0)$, is located. Generally, sheet $\Sigma_{-n}^{(2)}$ with $(n\geq 0)$ is symmetric to sheet $\Sigma_{n+1}^{(2)}$ with respect to the real g axis, and its image is symmetric with respect to the imaginary k axis to sheet image $\Sigma_{n+1}'^{(2)}$ [see Eq. (3.24)]. In Fig. 9 one can see the spiral asymptotic trajectory of the

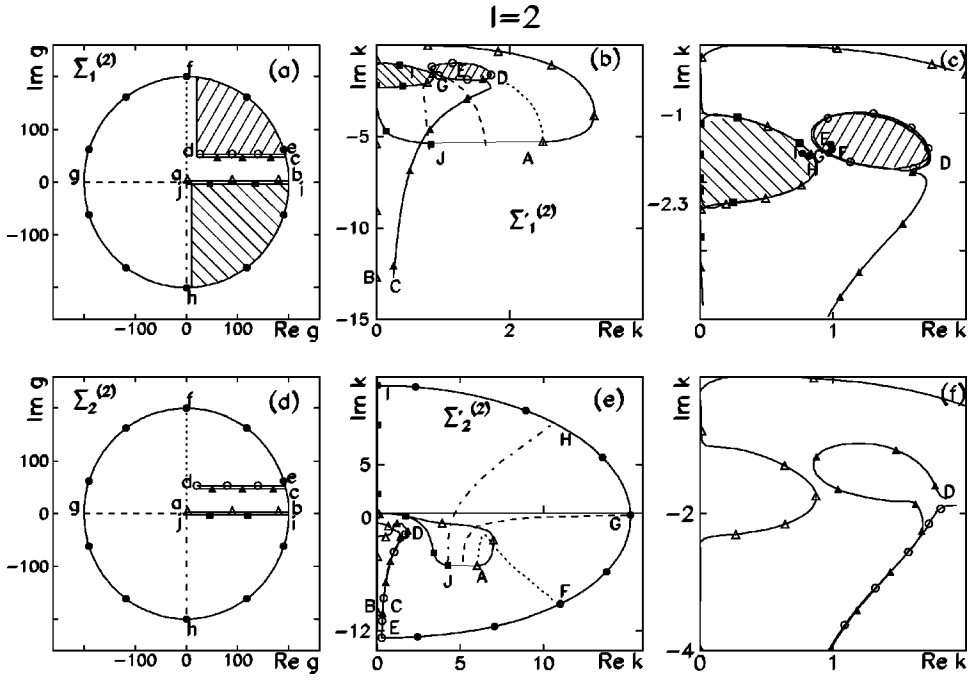

FIG. 8. Sheets $\Sigma_n^{(2)}(n=1,2)$ of the Riemann surface $R_g^{(2)}$ and their images $\Sigma_n'^{(2)}$ for a central rectangular potential with $l=2$. The sheet borders made of the edges of the cut $[0,\infty)$, the edges of the cuts that join the complex branch points, and a circle of a large radius are shown in (a) and (d). The k-plane images $\Sigma_1'^{(2)}$ and $\Sigma_2'^{(2)}$ are shown in (b) and (e). Details of these k-plane images are shown in (c) and (f). The hatched regions of sheet $\Sigma_1^{(2)}$ are mapped by the function $k=k^{(2)}(g)$ onto bound regions of sheet image $\Sigma_1'^{(2)}$ that are indicated by the same hatching. In each of these bound regions of $\Sigma_1'^{(2)}$ the exotic resonant state pole is situated. One can see that the region of the k-plane occupied by the exotic resonant state pole on sheet image $\Sigma_1'^{(2)}$ is empty on sheet image $\Sigma_2'^{(2)}$.

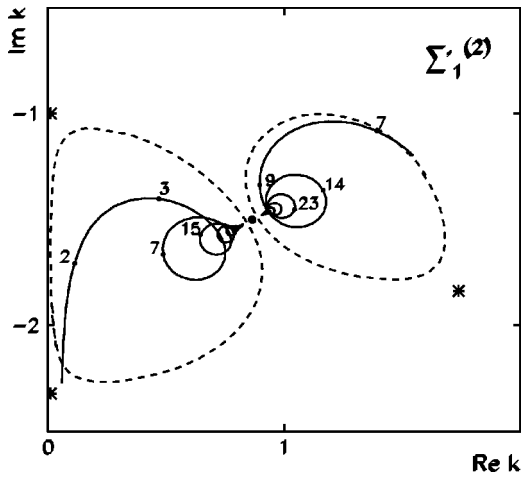

FIG. 9. The trajectories of the exotic resonant state pole on sheet image $\Sigma_1'^{(2)}$ for g varying as $g=\lambda(8+i)$ and as $g=\lambda(8-i)$, respectively, with λ taking values up to 200. The numbers beside the spiral curves give the λ values. We indicate the stable point by ● and the images of the branch points by ⋆.

exotic pole on $\Sigma_1'^{(2)}$ approaching the stable point $\kappa_1^{(2)}=0.866-1.5i$ for $|g|\to\infty$.

4. Case l=3

The pole equation in the case $l=3$ is

$$\frac{ik^4-6k^3-21ik^2+45k+45i}{k^3+6ik^2-15k-15i}$$

$$=\frac{(k_0^4-21k_0^2+45)\sin k_0+(6k_0^3-45k_0)\cos k_0}{(6k_0^2-15)\sin k_0-(k_0^3-15k_0)\cos k_0}. \tag{3.37}$$

For $l=3$, systems (3.7) and (3.8) become

$$h_4^{(1)}(k)=\frac{-ie^{ik}}{k}\left[1+\frac{10i}{k}-\frac{45}{k^2}-\frac{105i}{k^3}+\frac{105}{k^4}\right]=0, \tag{3.38a}$$

$$j_4(k_0)=-\frac{1}{k_0^5}[(k_0^4-45k_0^2+105)\sin k_0 + k_0(10k_0^2-105)\cos k_0] = 0 \tag{3.38b}$$

and

$$h_2^{(1)}(k)=\frac{ie^{ik}}{k}\left[1+\frac{3i}{k}-\frac{3}{k^2}\right]=0, \tag{3.38c}$$

$$j_2(k_0)=-\frac{3\cos k_0}{k_0^2}+\frac{(3-k_0^2)\sin k_0}{k_0^3}=0, \tag{3.38d}$$

TABLE IV. The branch points in the case $l=3$. The zeros of the spherical Bessel functions $j_2(k_0)$ and $j_4(k_0)$, respectively, are denoted by $k_{0,s}^-$ and $k_{0,s}^+$. $k_{s'}$ $(s'=1,2)$ stand for the zeros of the spherical Hankel function of the first kind $h_2^{(1)}(k)$, and $k_{s'}$ $(s'=3,4,5,6)$ stand for the zeros of the spherical Hankel function of the first kind $h_4^{(1)}(k)$.

s'	s	$k_{0,s}^-$	$k_{s'}$	$g_{s,s'}^-$
1	1	5.763	$0.866-1.500i$	$34.717+2.598i$
1	2	9.095	$0.866-1.500i$	$84.219+2.598i$
1	3	12.323	$0.866-1.500i$	$153.355+2.598i$
⋮	⋮	⋮	⋮	⋮
1	n	$\sim(n+1)\pi$	$\sqrt{3}/2-3i/2$	$\sim(n+1)^2\pi^2-k_1^2$
2	1	5.763	$-0.866-1.500i$	$34.717-2.598i$
2	2	9.095	$-0.866-1.500i$	$84.219-2.598i$
2	3	12.323	$-0.866-1.500i$	$153.355-2.598i$
⋮	⋮	⋮	⋮	⋮
2	n	$\sim(n+1)\pi$	$-\sqrt{3}/2-3i/2$	$\sim(n+1)^2\pi^2-k_2^2$
s'	s	$k_{0,s}^+$	$k_{s'}$	$g_{s,s'}^+$
3	1	8.183	$0.867-2.896i$	$74.590+5.023i$
3	2	11.705	$0.867-2.896i$	$144.641+5.023i$
3	3	15.040	$0.867-2.896i$	$233.827+5.023i$
⋮	⋮	⋮	⋮	⋮
3	n	$\sim(n+2)\pi$	$0.867-2.896i$	$\sim(n+2)^2\pi^2-k_3^2$
4	1	8.183	$-0.867-2.896i$	$74.590-5.023i$
4	2	11.705	$-0.867-2.896i$	$144.641-5.023i$
4	3	15.040	$-0.867-2.896i$	$233.827-5.023i$
⋮	⋮	⋮	⋮	⋮
4	n	$\sim(n+2)\pi$	$-0.867-2.896i$	$\sim(n+2)^2\pi^2-k_4^2$
5	1	8.183	$2.657-2.104i$	$64.319+11.181i$
5	2	11.705	$2.657-2.104i$	$134.368+11.181i$
5	3	15.040	$2.657-2.104i$	$223.556+11.181i$
⋮	⋮	⋮	⋮	⋮
5	n	$\sim(n+2)\pi$	$2.657-2.104i$	$\sim(n+2)^2\pi^2-k_5^2$
6	1	8.183	$-2.657-2.104i$	$64.318-11.181i$
6	2	11.705	$-2.657-2.104i$	$134.369-11.181i$
6	3	15.040	$-2.657-2.104i$	$223.556-11.181i$
⋮	⋮	⋮	⋮	⋮
6	n	$\sim(n+2)\pi$	$-2.657-2.104i$	$\sim(n+2)^2\pi^2-k_6^2$

respectively. In Table IV the values of the branch points and of their images in the k plane are presented.

The Riemann surface $R_g^{(3)}$ is constructed in the same manner as in the previous cases. Let $s=1,2,3,\ldots$. Sheet $\Sigma_s^{(3)}$ is joined with sheet $\Sigma_{s-1}^{(3)}$ at $g_{s,1}^-$. Sheet $\Sigma_{-s}^{(3)}$ is joined with sheet $\Sigma_{-s+1}^{(3)}$ at the branch point $g_{s,2}^+$. Sheet $\Sigma_0^{(3)}$ is joined with sheet $\Sigma_s^{(3)}$ at the branch point $g_{s,3}^+$. Sheet $\Sigma_0^{(3)}$ is joined with sheet $\Sigma_{-s}^{(3)}$ at the branch point $g_{s,4}^+$. Sheet $\Sigma_1^{(3)}$ is joined with sheet $\Sigma_{s+1}^{(3)}$ at $g_{s,5}^+$. Sheet $\Sigma_{-1}^{(3)}$ is joined with sheet $\Sigma_{-s-1}^{(3)}$ at $g_{s,6}^+$. The way the sheets are joined is shown schematically in Fig. 10. For simplicity, only the junctions of sheets $\Sigma_n^{(3)}$ and $\Sigma_m^{(3)}$ with $n,m\geqslant 0$ are shown.

In Fig. 11 sheets $\Sigma_0^{(3)}$, $\Sigma_1^{(3)}$, and $\Sigma_2^{(2)}$ and their k-plane

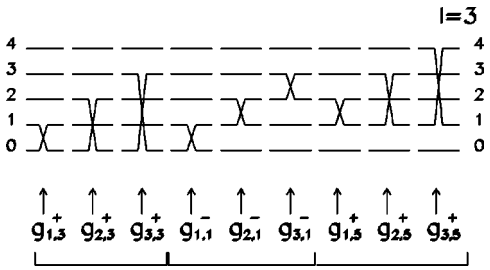

FIG. 10. The junctions of the sheets $\Sigma_n^{(3)}$ and $\Sigma_m^{(3)}$ $(n,m=0,1,2,3,4)$ for a central rectangular potential with $l=3$ at the branch points $g^-_{s,1}$, $g^-_{s,2}$, $g^+_{s,3}$, $g^+_{s,4}$, $g^+_{s,5}$, and $g^+_{s,6}$ $(s=1,2,3)$. The label n or m of each sheet is indicated by the numbers given at the left and right ends of the picture.

images are represented. One can see that on sheet $\Sigma_0^{(3)}$ there are four regions, indicated by hatching, corresponding to strong absorption $(\mathrm{Im}\,g>\mathrm{Im}\,g^+_{s,3})$, strong emission $(\mathrm{Im}\,g<\mathrm{Im}\,g^+_{s,4})$, weak absorption $(0<\mathrm{Im}\,g<\mathrm{Im}\,g^-_{s,1})$ and weak emission $(\mathrm{Im}\,g^-_{s,2}<\mathrm{Im}\,g<0)$, respectively, that are mapped by the function $k=k^{(3)}(g)$ on some bound regions of the k-plane sheet image $\Sigma_0'^{(3)}$. As the cuts on sheet $\Sigma_0^{(3)}$ are symmetric with respect to the real g axis, the bound regions on the corresponding k-plane image $\Sigma_0'^{(3)}$ are symmetric with respect to the imaginary k axis. Each of these bound regions where the exotic resonant state pole is located lies on a pair of points in the k plane: the image of a branch point and a stable point. For example, the bound region which occurs for strong absorption lies on the k-plane image of the branch point $g^+_{s,3}$ and on the stable point $\kappa_1^{(3)}=-2.322i$. The bound region which occurs for weak absorption lies on the image of the branch point $g^-_{s,1}$ and on the stable point $\kappa_2^{(3)}=1.754-1.839i$.

On sheet $\Sigma_1^{(3)}$ there are also two regions that correspond to strong absorption $(\mathrm{Im}\,g>\mathrm{Im}\,g^+_{s,5})$ and to emission $(\mathrm{Im}\,g<0)$, that are mapped by the function $k=k^{(3)}(g)$ on some bound regions on the k-plane sheet image $\Sigma_1'^{(3)}$. The bound region where the exotic resonant state pole is located for strongly absorptive potential lies on the k-plane image of the branch point $g^+_{s,5}$ and on the stable point $\kappa_2^{(3)}=1.754-1.839i$. For any absorptive potential the bound regions of the k plane, where the exotic resonant state pole was located on the sheet image $\Sigma_0'^{(3)}$, is empty on sheet image $\Sigma_1'^{(3)}$. Riemann sheet images $\Sigma_0'^{(3)}$ and $\Sigma_1'^{(3)}$ do not include the positive imaginary k axis, i.e., the poles on these sheet images cannot become bound state poles when the depth of the potential well is increased.

On $\Sigma_n'^{(3)}$ $(n\geqslant 2)$ there are only old-class resonant state poles. The bound regions where the exotic resonant state poles were located on $\Sigma_0'^{(3)}$ and $\Sigma_1'^{(3)}$ are empty on the sheets $\Sigma_n'^{(3)}$ $(n\geqslant 2)$. Sheets $\Sigma_n^{(3)}$ and $\Sigma_{-n}^{(3)}$ are symmetric

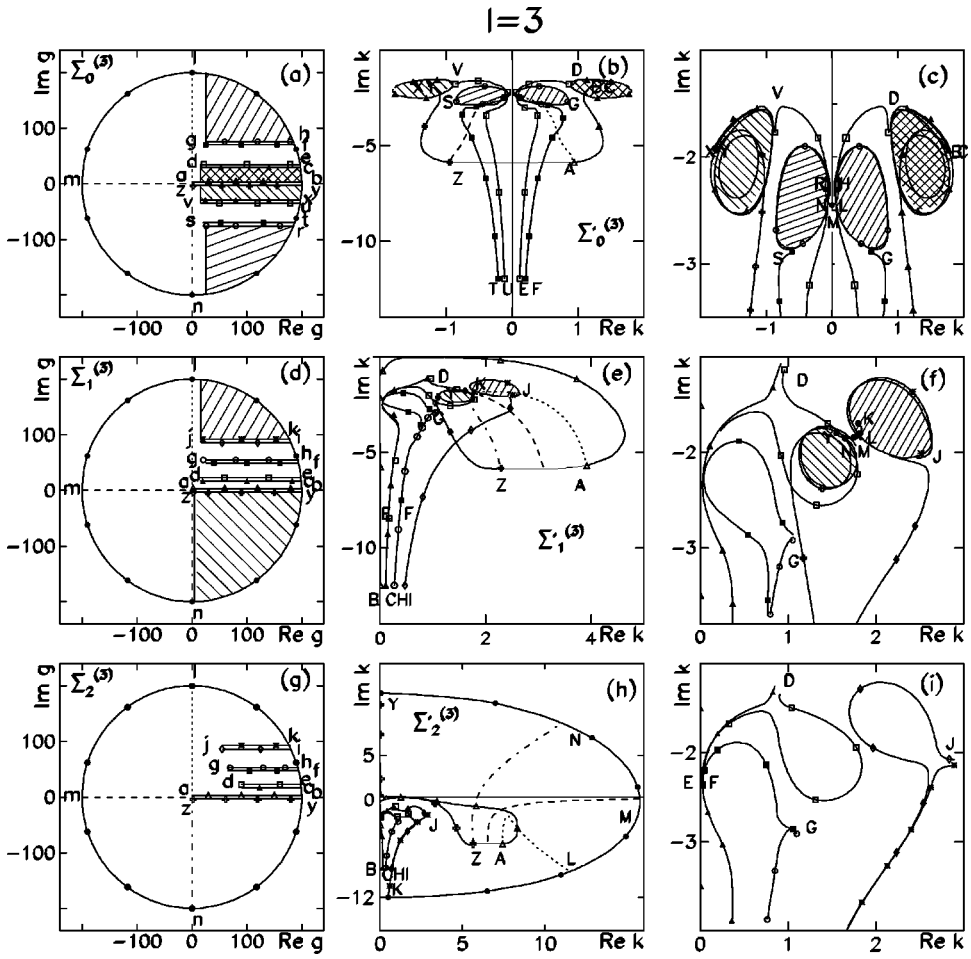

FIG. 11. Sheets $\Sigma_n^{(3)}$ $(n=0,1,2)$ of the Riemann surface $R_g^{(3)}$ and their images $\Sigma_n'^{(3)}$ for a central rectangular potential with $l=3$. The borders of the sheets made of the edges of the cut $[0,\infty)$, the edges of the cuts that join the complex branch points, and a circle of a large radius are shown in (a), (d), and (g). The corresponding k-plane images of the sheet borders are shown in (b), (e), and (h). Details of sheet images $\Sigma_0'^{(3)}$, $\Sigma_1'^{(3)}$, and $\Sigma_2'^{(3)}$ are shown in (c), (f), and (i). The hatched regions of sheet $\Sigma_0^{(3)}$ are mapped by the function $k=k^{(3)}(g)$ onto bound regions of the sheet image $\Sigma_0'^{(3)}$, indicated by the same hatching. Similarly, the hatched regions of sheet $\Sigma_1^{(3)}$ are mapped by the function $k=k^{(3)}(g)$ onto bound regions of sheet image $\Sigma_1'^{(3)}$, indicated by the same hatching. The k-plane region occupied on sheet images $\Sigma_0'^{(3)}$ and $\Sigma_1'^{(3)}$ by the exotic resonant state pole are empty on sheet image $\Sigma_2'^{(3)}$.

with respect to the real g axis, so that their k-plane images are symmetric with respect to the imaginary k axis.

5. Case l=4

The pole equation for $l=4$ is

$$\frac{k^5+10ik^4-55k^3-195ik^2+420k+420i}{ik^4-10k^3-45ik^2+105k+105i}=\frac{(10k_0^4-195k_0^2+420)\sin k_0-(k_0^5-55k_0^3+420k_0)\cos k_0}{(10k_0^3-105k_0)\cos k_0+(k_0^4-45k_0^2+105)\sin k_0}. \tag{3.39}$$

The branch points and their k-plane images are obtained by solving the system of equations (3.7) and (3.8), according to the procedure described for the cases $l=0$, 1, 2, and 3. In Table V the branch points and their k-plane images are given.

Let $s=1,2,3,\ldots$. Sheet $\Sigma_s^{(4)}$ is joined to sheet $\Sigma_{s+1}^{(4)}$ at the branch point $g_{s,1}^-$. Sheet $\Sigma_{-s}^{(4)}$ is joined to sheet $\Sigma_{-s+1}^{(4)}$ at the branch point $g_{s,2}^-$. Sheet $\Sigma_0^{(4)}$ is joined to sheet $\Sigma_{s+1}^{(4)}$, and sheet $\Sigma_0^{(4)}$ is joined to sheet $\Sigma_{-s-1}^{(4)}$ at the branch points $g_{s,3}^-$ and $g_{s,4}^+$. Sheet $\Sigma_1^{(4)}$ is joined to sheet $\Sigma_{s+1}^{(4)}$ at the branch point $g_{s,5}^+$. Sheet $\Sigma_0^{(4)}$ is joined to sheet $\Sigma_{-s}^{(4)}$ at the branch point $g_{s,6}^+$. Sheet $\Sigma_2^{(4)}$ is joined to sheet $\Sigma_{s+2}^{(4)}$ at the branch point $g_{s,7}^+$. Sheet $\Sigma_{-1}^{(4)}$ is joined to sheet $\Sigma_{-s-1}^{(4)}$ at the branch point $g_{s,8}^+$. In Fig. 12 the way the various sheets are joined at the branch points is shown. For simplicity, only the junctions of sheets $\Sigma_n^{(4)}$ and $\Sigma_m^{(4)}$ with $n,m\geqslant 0$ are shown.

In Fig. 13 sheets $\Sigma_1^{(4)}$, $\Sigma_2^{(4)}$, and $\Sigma_3^{(4)}$ and their k-plane images are shown. Sheets $\Sigma_{-n+1}^{(4)}$ and $\Sigma_n^{(4)}$ are symmetric with respect to the real g axis, so that their k-plane images are symmetric with respect the imaginary k axis, according to Eq. (3.24). One can see that there are four sheet images, namely, $\Sigma_{-1}'^{(4)}$, $\Sigma_0'^{(4)}$, $\Sigma_1'^{(4)}$, and $\Sigma_2'^{(4)}$, on which there are bound regions of the k plane where the exotic resonant state poles are located. On $\Sigma_1'^{(4)}$ there are three such bound regions: the first one corresponds to a strong absorption, i.e., to $\mathrm{Im}\,g>\mathrm{Im}\,g_{s,5}^+$; the second one corresponds to weak absorption, i.e., $0<\mathrm{Im}\,g<\mathrm{Im}\,g_{s,1}^-$; and the third one corresponds to an emissive potential $\mathrm{Im}\,g<0$. Each of these bound regions lies on one of the k-plane images of the branch points and on one of the stable points $\kappa_2^{(4)}=2.657-2.104i$ and $\kappa_1^{(4)}=0.867-2.896i$, which are zeros of $h_4^{(1)}(k)$ in the fourth quadrant of the k plane. In Figs. 13(b) and 13(c) the position in the k plane of the images of the branch points $g_{s,1}^-$ and $g_{s,5}^+$ are denoted by D and G, respectively. The positions of the images of the branch points $g_{s,3}^-$ and $g_{s,4}^+$, i.e., $k=-2.322i$ and $k=-3.647i$ are indicated.

On $\Sigma_2'^{(4)}$ there are also two bound regions where the pole is confined. One of these regions corresponds to $\mathrm{Im}\,g>\mathrm{Im}\,g_{s,7}^+$ (strong absorption), and the other to $\mathrm{Im}\,g<0$ (emission). The bound regions of the k plane where the exotic resonant state pole is confined on the sheet image $\Sigma_1'^{(4)}$ cannot be reached by the pole on the sheet image $\Sigma_2'^{(4)}$ if the potential is absorptive. The bound region where the exotic resonant state pole for absorptive potential is situated lies on the k-plane image of the branch point $g_{s,7}^+$, denoted by J in Figs. 13(e) and 13(f), and on the stable point $\kappa_2^{(4)}=2.657-2.104i$.

On sheet images $\Sigma_n'^{(4)}$ and $\Sigma_{-n+1}'^{(4)}$, $n\geqslant 3$, there are no exotic poles. Indeed, when the depth of the potential well increases the pole becomes a bound or virtual state pole, depending on the edge of the cut along the real axis on which the potential depth increases, as one can see from Fig. 13(h).

D. Properties of Riemann sheets $\Sigma_n^{(l)}$ and of their images $\Sigma_n'^{(l)}$ in the k plane

The global method used above leads to a unified approach to bound, virtual, and resonant states of a particle scattered by a central potential $gV(r)$, $g\in\mathbb{C}$, followed by a g-independent real barrier. If g takes values on a given Riemann sheet $\Sigma_n^{(l)}$, the corresponding pole belongs to the Riemann sheet image $\Sigma_n'^{(l)}$. The quantum numbers of the corresponding bound, virtual, or resonant state are (l,n). In this way, with a given state (l,n) we associate a Riemann sheet $\Sigma_n^{(l)}$. This association of a Riemann sheet to a state is an interesting insight into the intrinsic nature of the quantum state. This approach allows one to study not only each state (l,n), but also to understand the transition from state (l,n) to state (l,m) as a result of potential strength variation. Indeed, let us suppose that g describes a closed contour which starts from a point on sheet $\Sigma_n^{(l)}$ and encloses the branch point joining sheets $\Sigma_n^{(l)}$ and $\Sigma_m^{(l)}$. Then the pole passes from sheet image $\Sigma_n'^{(l)}$ to sheet image $\Sigma_m'^{(l)}$, i.e., the system makes a transition from state (l,n) to state (l,m), as a result of the potential strength variation. Here states (l,n) and (l,m) can be either bound or resonant states.

The new quantum number n is completely different in kind from l. While the orbital angular momentum l is related to the rotational invariance, the quantum number n has a topological meaning. It was for a long time thought that, since a pole in the lower half-plane will lead to a bound state if the potential well strength g is sufficiently increased, it could be labeled by the radial quantum number of the bound state. The labeling of resonant states by the radial quantum number of the bound states is not legitimate for the following reasons: (i) There are resonant state poles (exotic poles) that do not become bound state poles as the depth of the potential well increases; these poles could not be labeled by a radial quantum number of the bound states. (ii) The radial quantum number would change as the potential strength is varied, while we need a label which is independent on the potential strength. By introducing the new quantum number these shortcomings are removed. In the following the conclusions that can be drawn from the construction and analysis of Rie-

TABLE V. Branch points for $l=4$. The zeros of the spherical Bessel functions $j_3(k_0)$ and $j_5(k_0)$, respectively, are denoted by $k_{0,s}^-$ and $k_{0,s}^+$. $k_{s'}$ $(s'=1,2,3)$ stand for the zeros of the spherical Hankel function of the first kind $h_3^{(1)}(k)$ and $k_{s'}$ $(s'=4,5,6,7,8)$ stand for the zeros of the spherical Hankel function of the first kind $h_5^{(1)}(k)$.

s'	s	$k_{0,s}^-$	$k_{s'}$	$g_{s,s'}^-$
1	1	6.988	$1.754-1.839i$	$49.135+6.452i$
1	2	10.417	$1.754-1.839i$	$108.820+6.452i$
1	3	13.698	$1.754-1.839i$	$187.940+6.452i$
⋮	⋮	⋮	⋮	⋮
1	n	$\sim(n+3/2)\pi$	$1.754-1.839i$	$\sim(n+3/2)^2\pi^2-k_1^2$
2	1	6.988	$-1.754-1.839i$	$49.135-6.452i$
2	2	10.417	$-1.754-1.839i$	$108.820-6.452i$
2	3	13.698	$-1.754-1.839i$	$187.940-6.452i$
⋮	⋮	⋮	⋮	⋮
2	n	$\sim(n+3/2)\pi$	$-1.754-1.839i$	$\sim(n+3/2)^2\pi^2-k_2^2$
3	1	6.988	$-2.322i$	54.224
3	2	10.417	$-2.322i$	113.909
3	3	13.698	$-2.322i$	193.028
⋮	⋮	⋮	⋮	⋮
3	n	$\sim(n+3/2)\pi$	$-2.322i$	$\sim(n+3/2)^2\pi^2-k_3^2$
s'	s	$k_{0,s}^+$	$k_{s'}$	$g_{s,s'}^+$
4	1	9.356	$-3.647i$	100.830
4	2	12.967	$-3.647i$	181.430
4	3	16.355	$-3.647i$	280.775
⋮	⋮	⋮	⋮	⋮
4	n	$\sim(n+5/2)\pi$	$-3.647i$	$\sim(n+5/2)^2\pi^2-k_4^2$
5	1	9.356	$1.743-3.352i$	$95.730+11.683i$
5	2	12.967	$1.743-3.352i$	$176.330+11.683i$
5	3	16.355	$1.743-3.352i$	$275.675+11.683i$
⋮	⋮	⋮	⋮	⋮
5	n	$\sim(n+5/2)\pi$	$1.743-3.352i$	$\sim(n+5/2)^2\pi^2-k_5^2$
6	1	9.356	$-1.743-3.352i$	$95.730-11.683i$
6	2	12.967	$-1.743-3.352i$	$176.330-11.683i$
6	3	16.355	$-1.743-3.352i$	$275.675-11.683i$
⋮	⋮	⋮	⋮	⋮
6	n	$\sim(n+5/2)\pi$	$-1.743-3.352i$	$\sim(n+5/2)^2\pi^2-k_6^2$
7	1	9.356	$3.571-2.325i$	$80.183+16.603i$
7	2	12.967	$3.571-2.325i$	$160.783+16.603i$
7	3	16.355	$3.571-2.325i$	$260.128+16.603i$
⋮	⋮	⋮	⋮	⋮
7	n	$\sim(n+5/2)\pi$	$3.571-2.325i$	$\sim(n+5/2)^2\pi^2-k_7^2$
8	1	9.356	$-3.571-2.325i$	$80.183-16.603i$
8	2	12.967	$-3.571-2.325i$	$160.783-16.603i$
8	3	16.355	$-3.571-2.325i$	$260.128-16.603i$
⋮	⋮	⋮	⋮	⋮
8	n	$\sim(n+5/2)\pi$	$-3.571-2.325i$	$\sim(n+5/2)^2\pi^2-k_8^2$

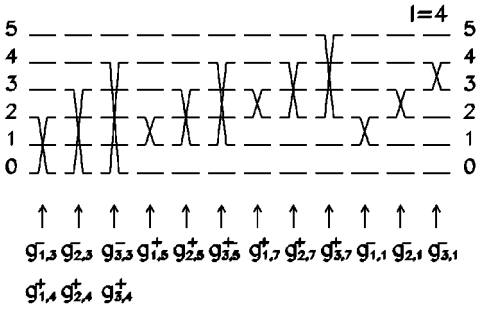

FIG. 12. The junctions of sheets $\Sigma_n^{(4)}$ and $\Sigma_m^{(4)}$ $(n,m=0,1,2,3,4,5)$ for a central rectangular potential with $l=4$ at the branch points $g_{s,1}^-$, $g_{s,2}^-$, $g_{s,3}^-$, $g_{s,4}^+$, $g_{s,5}^+$, $g_{s,6}^+$, $g_{s,7}^+$, and $g_{s,8}^+$, $(s=1,2,3)$. The label n or m of each sheet is indicated by the numbers given at the left and right ends of the picture.

mann sheets $\Sigma_n^{(l)}$ and their images $\Sigma_n'^{(l)}$ will be summarized.

1. Existence of the exotic resonant state poles

The new-class resonant state poles, also called exotic resonant state poles, exists provided that the potential well is followed by a barrier. In the absence of the barrier there is no exotic resonant state pole, as for example in the case of the central rectangular potential with $l=0$.

On sheet images $\Sigma_n'^{(l)}$, where $n=0,\pm1,\pm2,\ldots,\pm(l-1)/2$ for odd l and $n=0,\pm1,\pm2,\ldots,\pm(l-2)/2,l/2$ for even l $(l\neq0)$, there are bound regions where the exotic resonant state poles are located. The new-class poles do not become bound or virtual state poles as the potential strength g increases. The border of each bound region of the k plane where the exotic resonant state poles are situated lies on a pair of points: a stable point, and the k-plane image of a branch point. When the strength of the potential increases to infinity the exotic resonant state pole approaches the stable point [see Eq. (3.23)]. For a given l there are only l sheet images $\Sigma_n'^{(l)}$ that contain exotic resonant state poles. On these Riemann sheet images $\Sigma_n'^{(l)}$ $(l\neq0)$ there are no bound state poles. This is due to the fact that the exotic resonant state pole does not become a bound state pole when the depth of the potential well increases to infinity.

On each sheet image $\Sigma_n'^{(l)}$, with $n=0,\pm1,\pm2,\ldots,\pm(l-1)/2$ for odd l and $n=0,\pm1,\pm2,\ldots,\pm(l-2)/2,l/2$ for even l $(l\neq0)$, the pole can belong either to the new or old class of resonant state poles. There is an infinity of sheet images $[|n|>(l-1)/2$ for odd l and $n>l/2$, $n<-(l-2)/2$ for even $l\neq0]$ on which there are only old-class resonant state poles.

2. Absorption windows for the exotic resonant state poles

The cuts that are boundaries of a given sheet $\Sigma_n^{(l)}$ determine some threshold values for the imaginary part of the complex potential g. As we have already shown, there are $(2l+1)$ cuts for odd l and $(2l-1)$ cuts for even $l\neq0$, symmetrically distributed with respect to the real g axis. This means that there are l threshold values for the absorptive potential $(\mathrm{Im}\,g>0)$ when l is odd, and $l-1$ threshold values

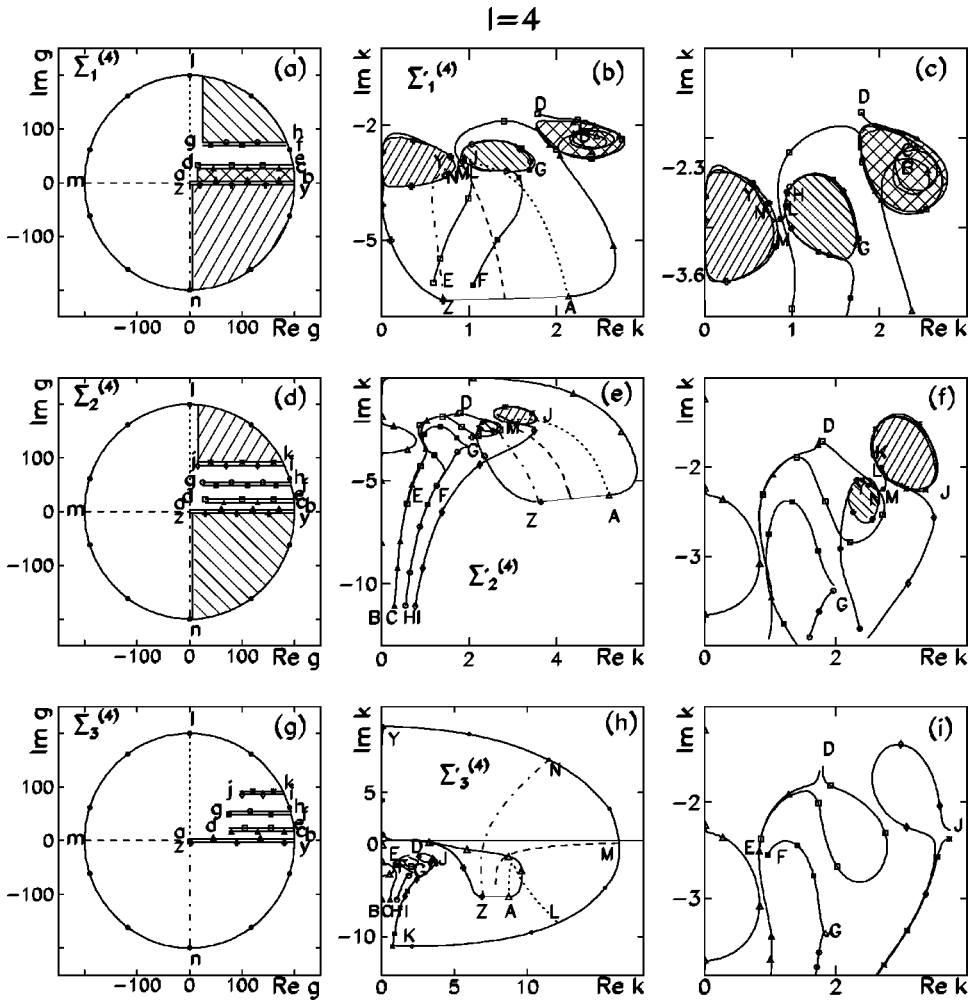

FIG. 13. Sheets $\Sigma_n^{(4)}$, $(n=1,2,3)$ of the Riemann surface $R_g^{(4)}$ and their k-plane images $\Sigma_n'^{(4)}$ for a central rectangular potential with $l=4$. The borders of the sheets made of the edges of the cut $[0,\infty)$, the edges of the cuts that join the complex branch points, and a circle of a large radius are shown in (a), (d), and (g). The corresponding k-plane images of the sheet borders are shown in (b), (e), and (f). Details of the k-plane images are shown in (c), (f), and (i). The regions of the Riemann sheets indicated by hatching are mapped by the function $k=k^{(4)}(g)$ onto bound regions in the corresponding k-plane sheet images, indicated by the same hatching. Each region occupied on sheet images $\Sigma_1'^{(4)}$ and $\Sigma_2'^{(4)}$ by the exotic resonant state pole are empty on sheet image $\Sigma_3'^{(4)}$.

for the absorptive potential when l is even and $l\neq 0$. For a given potential strength $g\in\Sigma_n^{(l)}$ the corresponding pole $k=k^{(l)}(g)$ on sheet image $\Sigma_n'^{(l)}$ belongs to the old or new class of resonant state poles. This depends on the sheet to which the given g belongs and on the value of $\mathrm{Im}\,g$ with respect to the thresholds on that sheet.

For the sake of simplicity, in the following we restrict our discussion to the absorptive thresholds. Taking into account the Jost function property (3.24), it is a simple matter to extend the results to the emissive potential as well.

For example, let l be odd. We denote by $(t_1<t_2<\cdots<t_l)$ the absorptive thresholds $(t_k=\mathrm{Im}\,g_{s,s'}^{\pm}>0)$. As shown, $\mathrm{Im}\,g_{s,s'}^{\pm}$ is constant for a given s' and arbitrary s. On sheet image $\Sigma_n'^{(l)}$ with $n=(l-1)/2$ the pole belongs to the new class of resonant state poles if $\mathrm{Im}\,g>t_l$ (strong absorption), and to the old class of resonant state poles if $0<\mathrm{Im}\,g<t_l$ (weak absorption). On each sheet image $\Sigma_n'^{(l)}$ with $n=(i-1)/2\geqslant 0$, $(i=1,3,5,\ldots,l-2)$ there are exotic resonant state poles for weak absorption $0<\mathrm{Im}\,g<t_i$ or for strong absorption $\mathrm{Im}\,g>t_{i+1}$. In the region $t_i<\mathrm{Im}\,g<t_{i+1}$ there are only old-class poles. On the sheet image $\Sigma_n'^{(l)}$ with $n>(l-1)/2$ there are only old-class poles for $0<\mathrm{Im}\,g<\infty$.

There is a similar situation for even l $(l\neq 0)$. On sheet image $\Sigma_n'^{(l)}$, with $n=l/2$, the pole belongs to the new class of resonant state poles if $\mathrm{Im}\,g>t_{l-1}$ (strong absorption) or to the old class of resonant state poles if $0<\mathrm{Im}\,g<t_{l-1}$ (weak absorption). On each sheet $\Sigma_n'^{(l)}$, with $n=i/2\geqslant 0$ $(i=2,4,\ldots,l-2)$, there are exotic resonant state poles for weak absorption $(0<\mathrm{Im}\,g<t_{i-1})$ or for strong absorption $(\mathrm{Im}\,g>t_i)$. In the region $t_{i-1}<\mathrm{Im}\,g<t_i$ there is an old-class pole. On sheet images $\Sigma_n'^{(l)}$, with $n>l/2$, there are only old-class poles.

The analysis of the Riemann sheets and of their k-plane images shows that the exotic resonant state poles (states) occur for a strong or weak absorption. While in the case of strong absorption the exotic resonant state poles occur for $l\geqslant 1$, in the case of weak absorption the exotic resonant state poles occur only for $l\geqslant 3$. This means that a higher real barrier is necessary for the occurrence of an exotic resonant state pole for a weak absorption. For example, for $l=2$ the exotic resonant state pole exists on $\Sigma_1'^{(2)}$ for strong absorption $(\mathrm{Im}\,g>\mathrm{Im}\,g_{s,4}^{+})$. For $l=3$ on $\Sigma_0'^{(3)}$ the exotic resonant state pole occurs for strong absorption $(\mathrm{Im}\,g>\mathrm{Im}\,g_{s,3}^{+})$ or for weak absorption $(0<\mathrm{Im}\,g<\mathrm{Im}\,g_{s,1}^{-})$. On $\Sigma_1'^{(3)}$ the exotic resonant state pole occurs for strong absorption $(\mathrm{Im}\,g>\mathrm{Im}\,g_{s,5}^{+})$.

In Fig. 14 we represent bound regions of the fourth quadrant of the k plane, where the exotic resonant state poles for

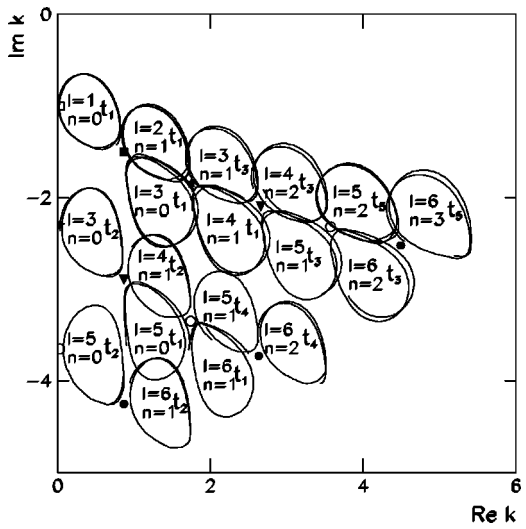

FIG. 14. The bound regions in the fourth quadrant of the k plane where the exotic resonant state poles for absorptive potential well are located for $l=1-6$. The regions of sheet images $\Sigma_n^{\prime(l)}$ on which the exotic resonant state pole occur are labeled by n, l, and t_i. By t_i the thresholds that define the absorption windows for the occurrence of the exotic resonant state poles are denoted. For a given l the thresholds are ordered according to the increasing imaginary part of the corresponding branch point. The boundary of each region is given by the pole trajectory corresponding to g going along the cut with $\mathrm{Im}\, g=\mathrm{Im}\, g_{s,s'}^{\pm}=t_i$. The positions of the stable points are indicated.

an absorptive potential well with $l=1-6$ are located. The label n of the sheet image is indicated. The boundary of each region is given by the pole trajectory corresponding to g going along the cut with $\mathrm{Im}\, g=\mathrm{Im}\, g_{s,s'}^{\pm}=t_i$. In other words, t_i denotes the threshold that defines the absorption window of the potential strength for the occurrence of the exotic resonant state pole. Here t_i can be either a strong absorption threshold or a week absorption threshold, according to the rules given above. The branch point image in the k plane is a transition point of the quantum system from the old-class resonant state to the new-class resonant state (exotic resonant state).

E. Properties of the exotic resonant states

1. Localization of the wave function of an exotic resonant state

The wave functions of the exotic resonant states corresponding to the exotic resonant state poles are mostly confined to the region outside the potential well. In order to characterize the localization of the wave functions in the case of potential (3.1), the contraction factor $dk^2/d(-g)$ defined by Lane [45] will be used.

Equation (3.4) can be written in the form

$$M_l(g,k)=\mathcal{L}_l^u-\mathcal{L}_l^w=0, \tag{3.40}$$

where the logarithmic derivatives $\mathcal{L}_l^u$ and $\mathcal{L}_l^w$ are defined by

$$\mathcal{L}_l^u=\frac{du_l(k_0,r)/dr}{u_l(k_0,r)}\Big|_{r=R=1}, \tag{3.41a}$$

$$\mathcal{L}_l^w=\frac{dw_l(k,r)/dr}{w_l(k,r)}\Big|_{r=R=1}, \tag{3.41b}$$

and $u_l(k_0,r)$ and $w_l(k,r)$ are the wave functions used in definition (3.3) of the Wronskian $W_l(g,k)$. Taking into account that the implicit function $k=k^{(l)}(g)$ is defined by Eq. (3.40), we calculate the derivative $dk^2/d(-g)=2kdk/d(-g)$:

$$\frac{dk^2}{d(-g)}=\frac{\partial M_l/\partial g}{\partial M_l/\partial k^2}=\frac{\partial \mathcal{L}_l^u/\partial g}{\partial \mathcal{L}_l^u/\partial k^2-\partial \mathcal{L}_l^w/\partial k^2}. \tag{3.42}$$

The derivatives $\partial \mathcal{L}_l^u/\partial k^2$ and $\partial \mathcal{L}_l^u/\partial g$ can be calculated by applying the method given in Ref. [46]. This gives

$$\frac{dk^2}{d(-g)}=\frac{\int_0^1 u_l^2 dr}{\int_0^1 u_l^2 dr+u_l^2(r=1)\partial \mathcal{L}_l^w/\partial k^2}. \tag{3.43}$$

The denominator of Eq. (3.43) is the square norm introduced by Schnol [47] for resonant states. This norm was first suggested by Zel'dovich [48] for $l=0$. According to Lane [45], we take $dk^2/d(-g)$ as an estimate of the wave-function localization. For bound states the second term in the denominator of Eq. (3.43) is negligible, so that we have $dk^2/d(-g)\sim 1$, which shows that the wave function is almost completely localized inside the potential well. Based on the recurrence relations (3.6a) and (3.6b), the numerator and denominator of Eq. (3.43) can be calculated. This gives

$$\frac{dk^2}{d(-g)}=\frac{k_0^2}{g}\frac{h_l^{(1)}(k)}{h_{l-1}^{(1)}(k)h_{l+1}^{(1)}(k)}-\frac{k^2}{g}. \tag{3.44}$$

Let $\kappa_n^{(l)}$ be a stable point, defined as a zero of $h_l^{(1)}(k)$. According to Eq. (3.23) the stable point acts as an attractor for the exotic resonant state pole, i.e., we have $k\to\kappa_n^{(l)}$ for $g\to\infty$. Consequently for $g\to\infty$ it results from Eq. (3.44) that $dk^2/d(-g)\to 0$ for the exotic resonant states. This means that for a sufficiently deep potential well the exotic resonant state pole is located in the neighborhood of the stable point $k=\kappa_n^{(l)}$ and, consequently, the corresponding exotic resonant state has a wave function almost completely confined to the region outside the potential well. As a consequence, the exotic resonant state is insensitive to the behavior of the potential in the region of the well, and is almost entirely determined by the geometric shape of the potential barrier.

2. Local degeneracy of the resonant levels corresponding to poles situated at the stable points

The resonant levels for the potential (3.1) exhibit a local degeneracy with respect to the orbital angular momentum l. We demonstrate that a resonant level (l,n) with orbital angular momentum l, defined by a pole situated at a stable

point $\kappa_i^{(l)}$, is degenerate with other resonant levels with orbital angular momenta $l-1$ and $l+1$. The stable point $\kappa_i^{(l)}$ is defined as the solution $k=\kappa_i^{(l)}$ of the equation $w_l(k,R)=0$, where $w_l(k,r)=krh_l^{(1)}(kr)$, and R is the radius of the central rectangular well. The distribution of the stable points in the k plane was discussed in Sec. III B. We recall that in the fourth quadrant of the k plane, including the negative imaginary axis, there are $i=(l+1)/2$ stable points for odd l and $i=l/2$ stable points for even l.

Let $g=\mathrm{g}_{i,p}^{(l)}$, $(p=1,2,\ldots)$ be the set of potential well strengths for which there is a resonant state of angular momentum l corresponding to a pole k situated at a stable point $\kappa_i^{(l)}$, i.e., for which $w_l(\kappa_i^{(l)},R)=0$. The values of $\mathrm{g}_{i,p}^{(l)}$ result from the condition of continuity of the wave function at the potential well radius:

$$u_l(\kappa_i^{(l)},R)=w_l(\kappa_i^{(l)},R)=0. \tag{3.45}$$

We will show that for $g=\mathrm{g}_{i,p}^{(l)}$ the S-matrix elements S_{l-1}, S_l, and S_{l+1} have a pole at the same position in the k plane, namely, at the stable point $k=\kappa_i^{(l)}$. In other words we will show that there is a local degeneracy with respect to l of the resonant levels with orbital angular momenta $l-1$, l, and $l+1$, provided that the potential well strength has a value that belongs to the discrete set $\mathrm{g}_{i,p}^{(l)}$, $(p=1,2,\ldots)$. Let k be a pole of the S_l-matrix element. This means that k satisfies Eq. (3.4), or equivalently, taking into account Eqs. (3.40) and (3.41),

$$\mathcal{L}_l^{(u)}(k,R)=\mathcal{L}_l^{(w)}(k,R). \tag{3.46}$$

By using the recurrence relations (3.6a) and (3.6b), satisfied by the solutions $u_l(k_0,r)$ at the stable point $\kappa_i^{(l)}$, and taking into account Eq. (3.45), it results that

$$\mathcal{L}_{l-1}^{(u)}(\kappa_i^{(l)},R)=b_l, \tag{3.47}$$

$$\mathcal{L}_{l+1}^{(u)}(\kappa_i^{(l)},R)=-b_{l+1}, \tag{3.48}$$

where $b_l=l/R$. Similarly, for $w_l(k,r)$,

$$\mathcal{L}_{l-1}^{(w)}(\kappa_i^{(l)},R)=b_l, \tag{3.49}$$

$$\mathcal{L}_{l+1}^{(w)}(\kappa_i^{(l)},R)=-b_{l+1}. \tag{3.50}$$

From Eqs. (3.47)–(3.50), we have

$$\mathcal{L}_{l-1}^{(u)}(\kappa_i^{(l)},R)=\mathcal{L}_{l-1}^{(w)}(\kappa_i^{(l)},R), \tag{3.51}$$

$$\mathcal{L}_{l+1}^{(u)}(\kappa_i^{(l)},R)=\mathcal{L}_{l+1}^{(w)}(\kappa_i^{(l)},R). \tag{3.52}$$

If $k=\kappa_i^{(l)}$ is a pole of the S-matrix element S_l for the strength of the potential well taking a value in the set $\mathrm{g}_{i,p}^{(l)}$ $(p=1,2,\ldots)$ defined by the equation $u_l(\kappa_i^{(l)},R)=0$, then, according to Eqs. (3.46), (3.51), and (3.52), it results that $k=\kappa_i^{(l)}$ is also a pole of the S-matrix elements S_{l+1} and S_{l-1} for the same value of the potential well strength. In fact $k=\kappa_i^{(l)}$ is the stable point of the function $k=k^{(l)}(g)$, a double pole of S_{l+1}, and a double pole of S_{l-1} [see Eqs. (3.7) and (3.8)]. It results that the above-mentioned system exhibits a local degeneracy with respect to the orbital angular momentum. More precisely, the resonant level with orbital angular momentum l defined by the pole at $\kappa_i^{(l)}$ is partly degenerate in l with the resonant levels with $l-1$ and $l+1$. Instead of the usual $(2l+1)$ degeneracy due to the spherical symmetry of the potential, the system has a $3(2l+1)$ degeneracy.

Let us consider the set of the Riemann surfaces $A=\{R_g^{(l)}\}$ $(l=0,1,2,\ldots)$, the set of sheets $B=\{\Sigma_n^{(l)}\}$ $(l=0,1,2,\ldots)$, and the set of sheet images $C=\{\Sigma_n'^{(l)}\}$ $(l=0,1,2,\ldots)$. According to the degeneracy demonstrated above, sheets $\Sigma_n^{(l)}$, $\Sigma_n^{(l-1)}$, and $\Sigma_n^{(l+1)}$ $(l>1)$, belonging to three distinct Riemann surfaces $R_g^{(l)}$, $R_g^{(l-1)}$, and $R_g^{(l+1)}$ from the set A, are joined at $g=\mathrm{g}_{i,p}^{(l)}$. Their images $\Sigma_n'^{(l)}$, $\Sigma_n'^{(l-1)}$, and $\Sigma_n'^{(l+1)}$ are joined at $k=\kappa_i^{(l)}$. We remark that these sheets, as well as their images, are distinct members of sets B and C, respectively. Taking this into account, two types of junctions are possible. The first one is the junction at the branch points $g=g_{s,s'}^{\pm}$ of the two sheets of the Riemann surface $R_g^{(l)}$. The second one is the junction at $g=\mathrm{g}_{i,p}^{(l)}$ of the sheets belonging to three distinct Riemann surfaces $R_g^{(l)}$, $R_g^{(l-1)}$, and $R_g^{(l+1)}$, respectively.

Due to this exact partial degeneracy there are three adjacent angular momenta that contribute to the resonant cross section. This result could seem surprising, because usually a resonance, i.e., a sharp change in the energy dependence of the cross section, occurs in a given l-wave partial cross section. Indeed the resonant-type structure disappears if the detector is placed at an angle equal to a zero of the corresponding Legendre polynomial $P_l(\theta)$. The increase of the cross section due to nonresonant phenomena can be distinguished from resonant phenomena by the fact that the former tend to result from the cooperative contribution from many partial waves [49]. In our case, due to the above-mentioned degeneracy, three partial cross sections $l-1$, l, and $l+1$ have resonant structures at the same energy, corresponding to that of the resonant state associated to the poles situated at the stable point $\kappa_i^{(l)}$. This is a new type of the resonance in the cross section which is associated with the contribution of the three partial waves. In Ref. [50] it was shown that the local degeneracy remains valid for exotic resonant levels in the case of a square well with a Coulomb barrier.

IV. CONCLUSIONS

An approach to bound and resonant states, based on a global analysis of S-matrix poles in the case of the scattering by a central potential $gV(r)$, $g\in\mathbb{C}$, followed by a g-independent real barrier, is presented. The Riemann surface $R_g^{(l)}$ over the g plane, on which the pole function $k=k^{(l)}(g)$ is single valued and analytic, is constructed. The Riemann surface $R_g^{(l)}$ is divided into sheets $\Sigma_n^{(l)}$, and the images $\Sigma_n'^{(l)}$ of these sheets in the k plane are constructed. If g takes values on a given Riemann sheet $\Sigma_n^{(l)}$, the pole $k^{(l)}(g)$ belongs to the Riemann sheet image $\Sigma_n'^{(l)}$ in the k plane. In this way the sheet $\Sigma_n^{(l)}$ of the Riemann surface $R_g^{(l)}$ is associated with a given state with quantum numbers (l,n).

From this we gain insight into the intrinsic nature of the quantum states. The Riemann surface approach to bound and resonant states, based on the global method for all *S*-matrix poles analysis, has several merits:

(1) Instead of analyzing an infinity of poles in the k plane, the global method allows one to analyze the single pole on each Riemann sheet image $\Sigma_n'^{(l)}$ in the k plane. Indeed, if the potential strength g takes a value on a given sheet $\Sigma_n^{(l)}$, then the function $k=k^{(l)}(g)$ takes only one value on the k-plane image $\Sigma_n'^{(l)}$ of the sheet; i.e., there is only a single pole on each sheet image. By analyzing each Riemann sheet image $\Sigma_n'^{(l)}$, no pole is lost.

(2) By the Riemann surface approach, to a given state (l,n) of the quantum system one associates a sheet $\Sigma_n^{(l)}$ of the Riemann surface $R_g^{(l)}$. This approach allows one not only to study each state (l,n), but also to understand the transition from state (l,n) to state (l,m) as a result of the potential strength variation. Indeed, let us suppose that g describes a closed contour which starts from a point on sheet $\Sigma_n^{(l)}$ and encloses the branch point joining sheets $\Sigma_n^{(l)}$ and $\Sigma_m^{(l)}$. Then the pole passes from sheet image $\Sigma_n'^{(l)}$ to sheet image $\Sigma_m'^{(l)}$, i.e., the system makes a transition from state (l,n) to state (l,m), as a result of potential strength variation. Here the states (l,n) and (l,m) can be either bound or resonant states. As a result a unified treatment of bound and resonant states is obtained.

(3) For a given potential form factor $V(r)$ the well and barrier with absorption or emission are treated simultaneously, which allows a smooth transition from one case to the other. Indeed, as g covers all the complex plane, each Riemann sheet $\Sigma_n^{(l)}$ for the potential $gV(r)$ contains a well and a barrier with absorption or emission. If g follows a continuous path on a given sheet $\Sigma_n^{(l)}$, then the corresponding pole follows a continuous path in the k-plane sheet image $\Sigma_n'^{(l)}$.

(4) A new quantum number n with topological meaning is introduced in order to label a pole and the corresponding state (l,n). Taking into account that on a Riemann sheet image $\Sigma_n'^{(l)}$ there is only one pole, the number n that labels the Riemann sheet $\Sigma_n^{(l)}$ and the Riemann sheet image $\Sigma_n'^{(l)}$ is used as a new quantum number for this pole and for the corresponding state (l,n).

(5) The global method for all *S*-matrix poles analysis is stable under the potential strength variation. Indeed, one cannot create or destroy *S*-matrix poles by varying the strength of the potential in the analyticity domain of the pole function $k=k^{(l)}(g)$. The poles can be created or destroyed only at the branch point $g=0$. If g follows a path on a sheet $\Sigma_n^{(l)}$, the corresponding pole describes a trajectory remaining on sheet image $\Sigma_n'^{(l)}$, provided that the path does not encircle a branch point and does not cross a small region containing the point $g=0$.

(6) The global method allows the identification of a new class of *S*-matrix poles (exotic poles) for the central rectangular potential with $l\neq 0$. The exotic resonant state poles and states have the following main properties.

(a) The exotic resonant state poles remain in the neighborhood of some special points called ''stable points'' when the strength of the potential well increases indefinitely ($k\rightarrow\kappa_n^{(l)}$ for $g\rightarrow\infty$). These exotic resonant state poles are insensitive to the behavior of the potential in the region of the well, and are almost entirely determined by the geometric shape of the potential barrier;

(b) The wave functions of the exotic resonant states are localized in the region of the barrier, rather than in the region of the well; the wave functions of the exotic resonant states that correspond to poles situated in the neighborhood of the stable points are almost completely confined to the region of the barrier;

(c) A resonant level (l,n) with orbital angular momentum l defined by a pole situated at the stable point $\kappa_i^{(l)}$ is degenerate with the resonant levels $(l-1,n)$ and $(l+1,n)$, where n is the new quantum number. Here each of the *S*-matrix poles $(l-1,n)$ and $(l+1,n)$ is a double pole. This degeneracy supports a new type of resonance in the cross section, associated with a cooperative contribution from three adjacent partial waves $l-1$, l, and $l+1$.

The global method is used in order to analyze all *S*-matrix poles for a central rectangular potential with $l=0$, 1, 2, 3, and 4. The construction of the Riemann surface $R_g^{(l)}$ is given in detail. The k-plane images of the sheets of the Riemann surface $R_g^{(l)}$ are analyzed.

It is expected that exotic resonant state poles to be present for any other potential shape consisting of a well followed by a barrier. For example, in Ref. [31] exotic resonant state poles were identified for a central rectangular or Woods-Saxon well with Coulomb and centrifugal barrier. A good candidate for the resonant states that correspond to such exotic poles are the quasimolecular states, evidenced in the study of nuclear heavy-ion reactions. These are resonant states with very special properties: (i) they are highly excited resonant states in nuclei, having energy in the neighborhood of the total (Coulomb plus centrifugal) barrier; (ii) they have good spins and parities (J^π); (iii) the widths Γ of these states are typically of the order of a few hundred keV; (iv) there are several quasimolecular states at each value J^π; and (v) the centroid of each group with the same J^π forms a straight line in the plane E_{exc} vs $J(J+1)$, appropriate to a rotational band. Feshbach [51] suggested that these quasimolecular states are fragments of a shape resonant state (parent quasimolecular state) with spin and parity J^π, having a width of the order of a few MeV. The fact that quasimolecular states have been observed in a region of high level density suggests that they belong to a new class of states of the nuclear system that fulfills extraordinary conditions to prevent them from spreading out. In Ref. [31] we showed that the parent quasimolecular states are exotic resonant states corresponding to the first stable point $\kappa_1^{(l)}$ for a central rectangular or Woods-Saxon well with a Coulomb and centrifugal barrier, that describes the scattering of two ions. The properties of the parent quasimolecular states [energies, widths, rotational character, deviation from the linear dependence of the energy on $J(J+1)$, doorway character, and criteria for observability] result natually from general properties of the exotic reso-

nant states. For example, the stability of the quasimolecular states against dissolution into the neighboring compound nuclear states is due to the localization of the exotic resonant state wave functions. Indeed, a parent quasimolecular state, being an exotic resonant state corresponding to a pole situated in the neighborhood of the stable point, has a wave function localized almost completely outside the potential well. This leads to a small overlap with adjacent compound nuclear states which are localized in a region having a radius smaller than the radius of the potential which describes the interaction of the two ions. Closed-form expressions for the energies and the widths of the parent quasimolecular states were given in Ref. [31]. A good agreement of the experimental and theoretical energies and widths was obtained without using any adjustable parameter.

ACKNOWLEDGMENTS

One of the authors (N.G.) is indebted to Professor C. J. Joachain for fruitful discussions.

[1] R. G. Newton, *Scattering Theory of Waves and Particles*, 2nd ed. (Springer-Verlag, New York, 1982).
[2] P. G. Burke, *Potential Scattering in Atomic Physics* (Plenum Press, New York, 1977).
[3] C. J. Joachain, *Quantum Collision Theory* (North Holland, Amsterdam 1975).
[4] J. Humblet and L. Rosenfeld, Nucl. Phys. **26**, 529 (1961).
[5] R. E. Peierls, Proc. R. Soc. London, Ser. A **253**, 16 (1959).
[6] K. M. McVoy, L. Heller, and M. Bolsterli, Rev. Mod. Phys. **39**, 245 (1967).
[7] G. Beck and H. H. Nussenzveig, Nuovo Cimento **18**, 416 (1960).
[8] H. H. Nussenzveig, Nuovo Cimento **20**, 694 (1961).
[9] D. N. Pattanyak and E. Wolf, Phys. Rev. D **13**, 2287 (1976).
[10] V. I. Kukulin, V. M. Krasnopol'sky, and J. Horáček, *Theory of Resonances* (Kluwer, Dordrecht, 1989).
[11] O. I. Tolstikhin, V. N. Ostrovsky, and H. Nakamura, Phys. Rev. A **58**, 2077 (1998).
[12] O. Latinne, H. J. Kylstra, M. Dörr, J. Purvis, M. Terao-Dunseath, C. J. Joachain, P. G. Burke, and C. J. Noble, Phys. Rev. Lett. **74**, 46 (1995).
[13] N. J. Kylstra and C. J. Joachain, Phys. Rev. A **57**, 412 (1998).
[14] W. J. Romo, Can. J. Phys. **52**, 1603 (1974).
[15] J. Bang, S. N. Ershov, F. A. Gareev, and G. S. Kazacha, Nucl. Phys. A **339**, 89 (1980).
[16] E. M. Ferreira and A. F. F. Teixeira, J. Math. Phys. **7**, 1207 (1966).
[17] E. M. Ferreira, N. Guilen, and J. Sesma, J. Math. Phys. **9**, 1210 (1968).
[18] H. M. Nussenzveig, Nucl. Phys. **11**, 499 (1959).
[19] S. Joffily, Nucl. Phys. A **215**, 301 (1973).
[20] P. Kaus and C. J. Pearson, Nuovo Cimento **28**, 500 (1963).
[21] L. P. Kok, Phys. Rev. C **22**, 2404 (1980).
[22] H. van Haeringen and L. P. Kok, Phys. Rev. C **24**, 1827 (1981).
[23] L. P. Kok and H. van Haeringen, Ann. Phys. (N.Y.) **131**, 426 (1981).
[24] W. Cassing, M. Stingl, and A. Weiguny, Phys. Rev. C **26**, 22 (1982).
[25] J. Dąbrowski, Phys. Rev. C **53**, 2004 (1996).
[26] H. Hogreve, Phys. Lett. A **201**, 111 (1995).
[27] A. Gal, G. Toker, and Y. Alexander, Ann. Phys. (N.Y.) **137**, 341 (1981).
[28] E. Oset, P. F. de Córdoba, L. L. Salcedo, and R. Brockman, Phys. Rep. **188**, 79 (1990).
[29] R. Bonetti, A. J. Koning, J. M. Accermans, and P. E. Hodgson, Phys. Rep. **247**, 1 (1994).
[30] R. M. DeVries, Comput. Phys. Commun. **11**, 249 (1976).
[31] C. Grama, N. Grama, and I. Zamfirescu, Ann. Phys. (N.Y.) **232**, 243 (1994).
[32] N. P. Erugin, *Implicit Functions* (Izdat. Leningradskogo Universiteta, Leningrad, 1956).
[33] A. I. Markuševič, *Theory of Analytic Functions* (Gosudarstv. Izdatel'stvo Tehniko-Teoretičeskoi Literatury, Moscow, 1950).
[34] R. G. Newton, J. Math. Phys. **1**, 319 (1960).
[35] W. J. Romo, J. Math. Phys. **20**, 1210 (1979).
[36] G. Julia, Soc. Math. France **54**, 461 (1926).
[37] S. Stoilow, *Lecons sur les Principles Topologiques de la Théory des Fonctions Analitiques* 2nd ed. (Gautier-Villars, Paris, 1956).
[38] H. Cartan, Bull. Sci. Math. **55**, 24 (1931).
[39] H. A. Antosiewicz, in *Handbook of Mathematical Functions with Formulas, Graphs and Mathematical Tables*, edited by M. Abramovitz and I. A. Stegun, Applied Mathematics Series Vol. 55 (U.S. GPO, Washington, DC, 1970), p. 435.
[40] V. N. Kublanovskaia and T. N. Smirnova, Trudy Mat. Inst. Steklova **53**, 186 (1959).
[41] E. M. Wright, Proc. R. Soc. Edinburgh, Sect. A: Math. Phys. Sci. **65**, 193 (1958/1959).
[42] E. Grosswald, *Bessel Polynomials* in Lecture Notes in Mathematics Vol. 698 (Springer-Verlag, New York, 1978).
[43] R. E. O'Malley Jr., Commun. Math. Inst. Rijksuniversiteit, Utrecht **5**, 2 (1977).
[44] F. W. J. Olver, in *Handbook of Mathematical Functions with Formulas, Graphs and Mathematical Tables* (Ref. [39]), p. 355.
[45] A. M. Lane, Phys. Lett. **33B**, 274 (1970).
[46] G. E. Brown, J. H. Gunn, and P. Gould, Nucl. Phys. **46**, 589 (1963).
[47] E. E. Schnol, Teor. Mat. Fiz. **8**, 140 (1971) [Theor. Math. Phys. **8**, 729 (1971)].
[48] Ya. B. Zel'dovich, Zh. Éksp. Teor. Fiz. **39**, 776 (1960) [Sov. Phys. JETP **12**, 542 (1961)].
[49] E. Gerjuoy, in *Autoionization*, edited by A. Temkin (Mono Book Corp., Baltimore, Maryland, 1966), p.33.
[50] C. Grama, N. Grama, and I. Zamfirescu, Europhys. Lett. **39**, 353 (1997).
[51] H. Feshbach, J. Phys. (Paris) Colloq. **5**, C-37 (1976).